INVESTIGATING THE EFFECT OF METALLIC NANOPARTICLES PRESENCE ON SIGNAL INTENSITY FOR DRIED-DROPLET ANALYSIS BY LASER-INDUCED PLASMA SPECTROSCOPY

A Thesis Submitted to
the Graduate School of Engineering and Sciences of
İzmir Institute of Technology
In Partial Fulfillment of the Requirements for the Degree of

MASTER OF SCIENCE

in Chemistry

by

Özge TETİK KARABIYIK

July,2021

İZMİR

ACKNOWLEDGMENTS

I would like to express my gratitude to the few people who have always been with me and always supported me during my thesis work.

First of all, I would like to thank my supervisor Prof. Dr. Şerife YALÇIN, who gave me the opportunity to work together. I am grateful for always encouraging me and supporting my ideas.

I would like to thank all committee members for their advice.I would also like to thank my lab friend Dilara Durkan for her support, friendship, and all the pleasant moments we had.

Also for great assistance in nanoparticle synthesis I would like to thank Dr. Sinan Balcı and his student Sema Sarısözen and all other lab members.

I would also like to thank Burak Karabıyık, who has always been with me in every aspect of my life. I would like to thank my mother Cavidan Tetik and my father Engin Tetik, who always showed their support for me, always stood by me, and strived for me to be an educated and strong woman. I would like to present the most special thanks to my grandmother Aliye Tetik and my grandfather Mehmet Tetik, who brought me to this day.

I dedicate this work to my grandfather. Rest in peace...

ABSTRACT

INVESTIGATING THE EFFECT OF METALLIC NANOPARTICLES PRESENCE ON SIGNAL INTENSITY FOR DRIED-DROPLET ANALYSIS BY LASER-INDUCED PLASMA SPECTROSCOPY

While solid sample analysis by LIBS is more easy and straightforward, liquid analysis is more troubling. One of the studies aimed at removing the problems in liquid analysis is the Nanoparticle Enhanced LIBS technique.

This study aims to investigate the effect of the presence of Ag nanoparticles of different shape and absorption wavelengths on the signal strength of heavy metals Pb and Cr. For that purpose, spherical, prism, and disc-shaped silver nanoparticles with an absorption wavelength in the range of 394-761 nm were used.

Among all types of NPs with different sizes and shapes, silver nanoparticles with an absorption maximum at 535 nm were found to enhance LIBS signal intensity of Pb element at 405.8 nm 5-6 times, and that of Cr at 428.9 nm 3-3.5 times. Under optimized conditions, a LOD value of 1,16 and 0.69 ppb were obtained for Pb and Cr, respectively. The applicability of the system for the determination of Pb and Cr in aqueous environments has also been tested on reference water samples.

The silver nanoparticle with an maximum absorbance wavelength of 535 nm shows the most improvement in signal. The wavelength of the laser used is very close to the absorbance wavelength of the silver nanoparticle, effectively overlapping it. Thanks to the transmitted laser light, plasmons are formed on the nanoparticle surface. These formed surface plasmons interact with the laser electromagnetic field, resulting in an increase in the signal.

ÖZET

LAZER-OLUŞTURMALI PLAZMA SPEKTROSKOPİSİ İLE KURUTULMUŞ DAMLACIK ANALİZİNDE METAL NANOPARÇACIK VARLIĞININ SİNYAL ŞİDDETİ ÜZERİNDEKİ ETKİSİNİN ARAŞTIRILMASI

LIBS tekniği ile her ne kadar katı maddenin analizi rahat ve kolay olsada sıvı örneklerle çalışılırken bazı problemler ortaya çıkmaktadır. Sıvı analizlerinde yaşanan bu problemleri kaldırmaya yönelik çalışmalardan biri nanoparçacık ile güçlendirilmiş LIBS tekniğidir.

Bu çalışmanın amacı Pb ve Cr ağır metali içeren solüsyonların LIBS ile analizinde farklı dalga boylarında absorbansa ve farklı şekillere sahip gümüş metal nanoparçacık varlığının LIBS sinyal şiddetine etkisinin araştırılmasıdır. Bu amaçla küresel, prizma ve disk şeklinde ve absorbans dalga boyları 394 ile 761 nm arasında değişen gümüş nanoparçacıklar kullanılmıştır.

Şekilleri ve dalgaboyları farklı olan tüm gümüş nanoparçacıklar içerisinde 535 nm'de maximum absorbansa sahip prizma şekilli gümüş nanoparçacık Pb LIBS sinyallerinde 5-6 kat oranında, Cr LIBS sinyallerinde ise 3-3,5 kat oranında iyileşme sağlayarak en yüksek iyileştirmeyi sağlayan gümüş nanoparçacık olmuştur. Optimize edimiş koşullar altında Pb tespit limiti 1.16 ppb, Cr tespit limiti ise 0.69 ppb bulunmştur. Ayrıca yöntemin kullanılabirliği için referans su örnekleri ile çalışmalar gerçekleştirilmiştir.

535 nm'de maximum absorbans dalga boyuna sahip gümüş nanoparçacık, sinyalde en fazla gelişmeyi gösterrmiştir. Kullanılan lazerin dalga boyu ile gümüş nanoparçacığın absorbans dalga boyu birbirine çok yakındır ve güçlü bir şekilde birbirleri ile etkinleşirler. İletilen lazer ışığı sayesinde nanoparçacık yüzeyinde plazmonlar oluşur. Oluşan bu yüzey plazmonları lazer elektromanyetik alanı ile etkileşerek sinyalde bir artışa neden olur.

TABLE OF CONTENTS

LIST OF FIGURES

Figure **Page**

Figure **Page**

Figure **Page**

Figure **Page**

LIST OF TABLES

Table **Page**

LIST OF ABBREVIATIONS AND SYMBOLS

LIBS	Laser-Induced Breakdown Spectroscopy
NELIBS	Nanoparticle Enhanced Laser-Induced Breakdown Spectroscopy
ICDD	Intensified Charge Coupled Detector
Nd:YAG	Neodymium-Yttrium Aluminum Garnet
DLS	Dynamic Light Scattering
NIST	National Institute of Standards and Technology
DL	Detection Limit
S/N	Signal-to-Noise-Ratio
ppb	part per billion
ppm	part per million
pg	picogram
μL	microliter
μs	microsecond
ns	nanosecond
mj	milli-Joule
mL	milliliter
L	liter
λ	wavelength
m	slope
nm	nanometer
t_d	Delay Time
t_g	Gate Time
Pb	Lead

Cr	Chromium
Ag	Silver
Au	Gold
AgNP	Silver Nanoparticle
Si_3N_4	Silicon Nitride
σ	Standard Deviation
WHO	World Health Organization
HPS	High Purity Standars
HPS-DWPS	High Purity Standars Drinking Water Metal Solution
SD	Standard Deviation

CHAPTER 1

INTRODUCTION

1.1 Laser Induced Breakdown Spectroscopy (LIBS)

Laser-Induced Breakdown Spectroscopy, LIBS is an atomic emission spectroscopic technique that uses extremely energetic laser pulses to stimulate optical excitation on the sample (Anabitarte et al, 2012).

In this technique, an energetic laser pulse focused on the sample (solid, liquid, or gas) with the help of a focusing lens then the forming of plasma on the sample surface by vaporizing a small amount of a sample. The emission from plasma collected by the convenient optics and transfer to the spectrograph. Emission signals are recorded by the detector and results are analyzed by the electronic display (Cremers and Radziemski, 1985).

As a simple, fast, and cost-effective method LIBS can be used range with minimum sample preparation steps, in any environment, all kinds of sample types; solids, liquids, and gases. It has been used in a variety of field including; cultural heritage (Gaudiuso et al., 2010, Tzortzakis, 2006), different diesel engine passenger vehicles (Viskup et al., 2020), industrial applications (Gallou et al., 2011), neuro-genetic approach (Nunes et al., 2010), civilian and military applications (Miziolek et al., 2008), environmental areas (Snesi et al., 2009), aerosol analysis (Dalyander et al., 2008), classification of polymer (Vinicius et al., 2017), microanalysis applications (Godwal et al., 2008), biomedical and geological fields (Jolivent et al., 2019).

1.1.1 Theory

The LIBS technique is an analytical technique based on measuring the emission of electromagnetic radiation released by the excitation of atoms or ions in a sample by laser light. The sample can be solid, liquid, or gas (Musazzi et al., 2014). The high-temperature plasma created by the short pulse laser sent on the sample is the main physical event of the LIBS technique. This short laser pulse sent to the sample causes some parts of the sample to decrease in volume. This process is called the ablation process. Figure 1.1 shows the ablation process in the LIBS analytical technique.

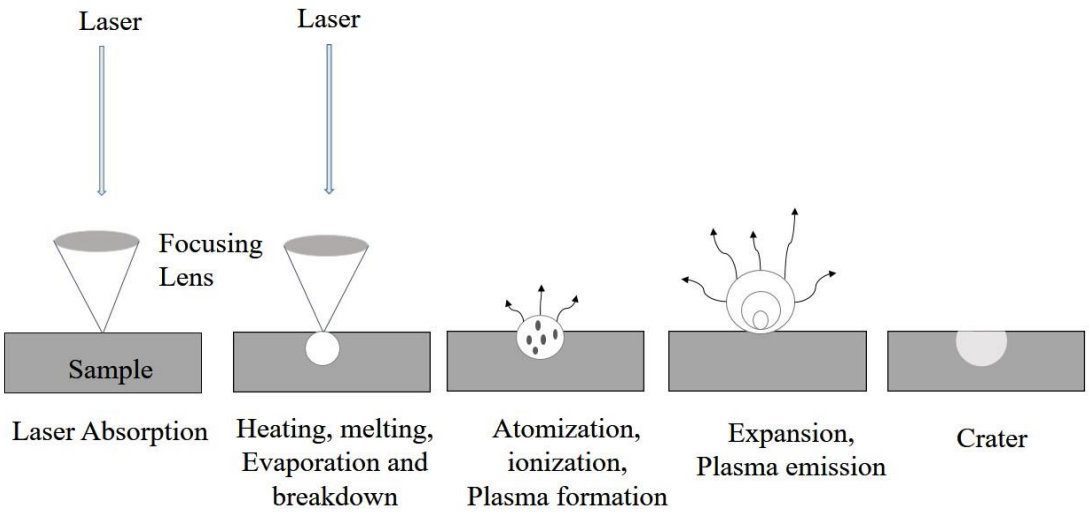

Figure 1.1. Ablation process in the LIBS technique

(Musazzi et al., 2014)

When the laser pulse is over, the laser begins to cool. Atoms and ions that are stimulated during the cooling of the plasma return from excited energy levels to ground state energy levels. This process is shown in Figure 1.2.

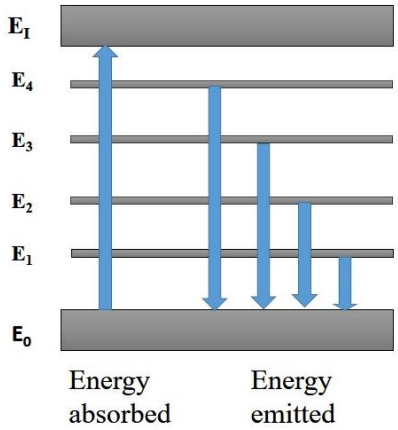

Figure 1.2. Absorption of laser light and emission of discrete atomic lines

As a result of this, excited atoms/ions in the plasma emits light at their characteristic wavelength. With the help of the ICDD / spectrograph detector, light emitted from the plasma is collected. Each element in the periodic table has its own characteristic emission lines, and these characteristic emission lines make possible the elemental analysis of the items. Besides, the signal intensities of LIBS peaks are useful in analyzing the elements in trace amounts in the sample. Figure 1.3 shows that the typical LIBS spectrum in the 200–820 nm range.

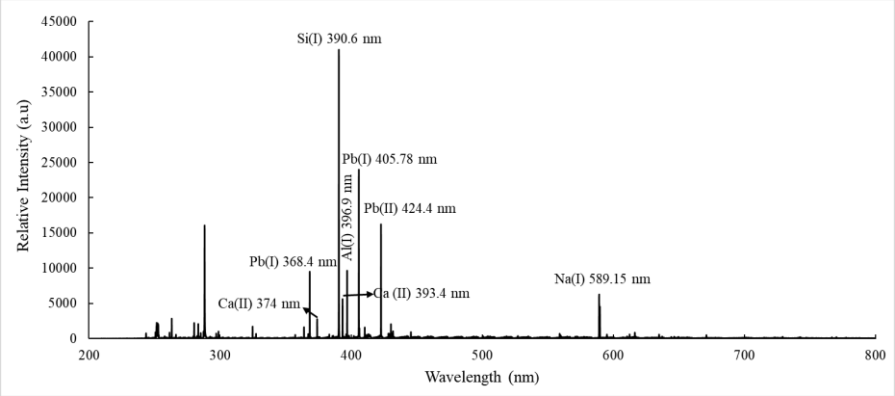

Figure 1.3. Typical LIBS spectrum in the 200–820 nm range.

1.1.2 Plasma

Since 1920, light-emitting plasmas have managed to be among the topics of science (Stimulated emission). Since 1960, laser-induced plasmas have begun to be studied (Rubby laser, CO_2 laser)(Jeff, 2010). The local combination, where

atoms, ions, and electrons, which are generally electrically neutral, act collectively, is called plasma (Cremers and Radziemski,1985).

Several parameters express plasma, the most fundamental of which is the degree of ionization. Plasmas with an electron ratio of less than 10% are called weakly ionized plasmas, while plasmas that have high electron-atom / ion ratios by stripping from electrons are called high ionized plasmas. LIBS plasmas are weakly ionized plasmas. The temporary history of LIBS plasma created with a single laser pulse is shown in figure 1.4.

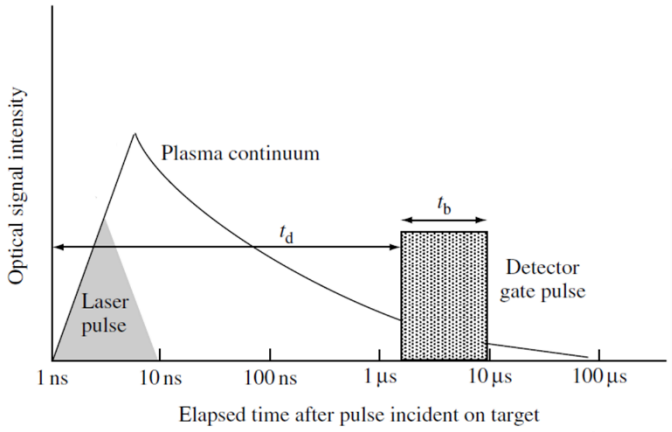

Figure 1.4. A general view of the temporal history of a LIBS plasma (Cremers and Radziemski, 2006).

Looking at the figure 1.4, it is seen that ionization is high in the early times. Electron-ion recombination, neutral atoms, and molecules are formed, respectively. Looking at the timeline in Figure 1.4, it can be seen that ions are formed from a pulse duration of 10 ns to about 5 ms. It is known that neutral atoms are formed between about 1 ms and 50 ms and finally the molecular part is formed after 10 ms.Continuity is ensured thanks to Bremsstrahlung (free–free) and recombination (free–bound) events. Electrons that accelerate or slow down during collisions allow the photons in the Bremsstrahlung process to emit. For recombination to occur, a free electron must reach the ionic or atomic energy level. The resolution of the plasma light with time allows discrimination of the dominant signals in LIBS.

While the delay from the initiation of the laser to the reception of the signal is indicated by t_d, how long the detector will remain on is indicated by t_b. The time scales shown in Figure 1.4 are for a plasma initiated at 1 atm with a laser pulse of 5 to 10 ns 1064 nm from an Nd: YAG laser. For longer pulsed lasers such as the CO_2 laser or shorter pulses such as pico or femtoseconds, this time scale expands or contracts. When the ambient pressure decreases, the energy absorbed in the plasma volume is less compressed and recycled, thus decreasing the life of the plasma (Cremers and Radziemski, 2006).

Typical plasma radiation processes are shown in these equations ; $V = \Delta E/h$,
$\bar{\nu} = \nu/c$, $\lambda = 1/\bar{\nu}$, when E is given in joules, the frequency, wave number, and wavelength of a transition are where ΔE is an energy level difference.

The relationship between spectral line characteristics and plasma properties is an important subject for the main diagnosis of plasma. Plasma temperature and electron density affect line widths, while line widths and shifts also affect the expansion mechanism. Dominant broadening mechanisms are used to determine spectral line profiles. The collision broadening mechanism is used to determine the collision effect of neutral atoms or molecules.

The Stark broadening mechanism happens by the collision of ions and electrons. Doppler broadening and Stark effect contribute to the line width provided that it is under normal LIBS conditions. The absolute temperature and atomic mass of the emitting species affect the Doppler broadening. The electric field in the plasma causes the Stark effect. The electric field in plasma is primarily caused by the collision of electrons. As the atomic mass increases, the Doppler broadening becomes smaller and the Stark broadening becomes dominant. Shifts in wavelengths, except for the high f level, will be less than 0.1 nm. Depending on the optical and spectral resolving power of the spectrometer-detector system, stark widths and shifts in plasma can be observed.

Another issue after line profile and line width is plasma opacity. The spread of the plasma is optically thin. Especially on the most intense line, if there is self-absorption, a value different from the expected value is obtained. There are two ways to check the optical thickness of a plasma. Depending on the strong spectral

lines of the elements, sometimes the optical thickness of the plasma can be determined experimentally, sometimes with the help of the atomic physics coupling theory. Verification can be made by checking the triple emission peaks of 777.19 nm, 777.42 nm, ad 777.64 nm of the O atom (Siemonsson and Miziolek, 1993). In another method, a round mirror is placed behind the plasma and line widths are compared with and without mirror (Bekefi, 1976).

Plasma definition is the definition of the properties that occur with the combination of molecules, electrons, and ions rather than the individual species. If there is thermodynamic equilibrium, the relative population of energy levels and the velocity distribution of particles can be used to explain the properties of the plasma. Local thermodynamic equilibrium definition is used within the definition of thermodynamic equilibrium. The idea is that balance occurs in small areas of the field, there may be changes in balance from region to region.When enough collisions occur, the energy in the plasma spreads across the volume and species, and heat is released from the plasma. Even in this state, not all species may be in thermodynamic equilibrium. Basic physics explains this by sharing the colliding particles in their energy according to their mass ratios. If conditions are at atmospheric pressure and an irradiance greater than $108 W/cm^2$ LIBS plasma becomes thermal a few hundred seconds after its initiation.

1.1.3 Instrumentation

The LIBS system has a simple experimental setup that is not complicated. The instrumentation can be summarized as described in Figure 1.5 as a short energy pulsed laser source (typically ranging from the nanosecond to femtosecond time scale), a focusing lens, collecting optics for the emitted radiation, a spectrograph, a detector, and a computer. It is a practical analytical method to generate analytical information by sending a single laser pulse on a sample.

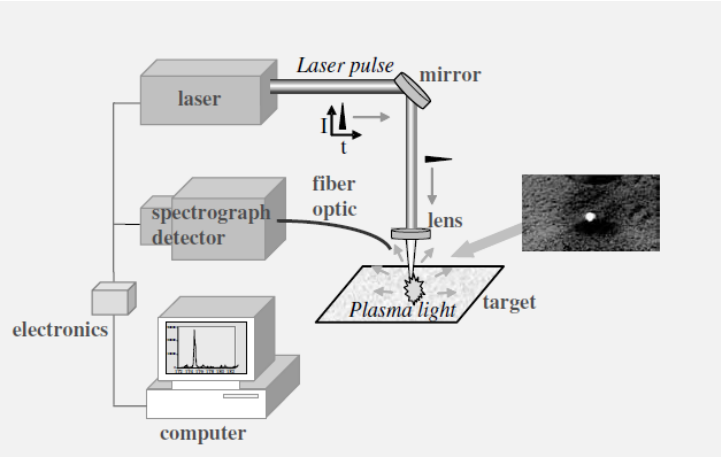

Figure 1.5. A typical LIBS set-up

(Cremers and Radziemski, 2006)

To produce plasma in all kinds of materials, only high-energy pulsed lasers are used in experiments with LIBS. There are different types of pulsed laser produced on the market for different techniques. Laser characteristic properties are a parameter that changes according to the behavior and quality of the plasma that the laser forms. These characteristics also affect LIBS measurements. At this point, many physical parameters in laser-matter interaction are affected such as wavelength, laser pulse duration, laser pulse energy, and beam quality. In general, the selection of the appropriate laser source varies according to the process to be performed. The laser intensity is a power per unit area (W cm^{-2}). If lasers are short-duration (nanosecond and femtosecond) pulses, it is possible to achieve the density per unit area at high watts such as billion or trillion watts. In addition, in the LIBS experiment set-up, the amount of intensity per unit area can be adjusted with the focus optics of the light hitting the sample. Thanks to this feature, the laser light focused on the target at a very small point can generate high power density. Monochromaticity of the laser and frequency spread of the impinging radiation is not very critical parameters. The most important point is here plasma formation is particularly on laser density.

Other important laser properties are the laser wavelength and pulse duration parameters called the beam quality factor. The interaction between the substance and laser largely depends on the beam quality factor. Electron production and growth due to collision ionization and multiple photon absorption also depend on the excitation wavelength. Collision-induced ionization occurs when long-

wavelength lasers are used, and multiple photon ionization occurs when short-wavelength lasers are used. The laser pulse duration, expressed by the full width at half maximum (FWHM), is effective during the formation of the plasma. In this case, it helps to determine the spectroscopic quantities. The pulse energy of picosecond lasers in the sample is lower than nanosecond lasers due to thermal diffusion. The reason for this is that when picosecond lasers are used, low radiation effects on substance interaction times and high transmitted irradiation. When femtosecond lasers are used with high radiation, it is possible to analyze with low ablation threshold energy since the pulse duration is very short. Today, it is possible to find laser sources with different wavelengths (ranging from UV to IR) and pulse times (ranging from microsecond to femtosecond) (Musazzi et al., 2014).

Laser sources with different properties are used in LIBS experiments from past to present. Some common laser sources are listed in table 1.1 (Musazzi et al., 2014).

Table 1.1. Laser sources list in LIBS experimental. Depends on both the pulse duration and the pulse repetition rate

(Musazzi et al., 2014).

Laser type	***Wavelength (nm)***	***Pulse duration (ns)***	***Energy/pulse (mJ)***
CO2 Q-Switched	10.6×10^3	200	100
Er: YAG Q-switched	2.94×10^3	170	25
Nd: YAG	1.064×10^3	4–10	0.1–3
Nd: YAG second harmonic	532	4–8	0.05–2
Nd: YAG third harmonic	354.7	4–8	0.02–0.7
Nd: YAG fourth harmonic	256	3–5	0.01–0.3
Ruby Q-switched	694.3	5–30	1–50
Ruby ps pulse	694.3	10-2	0.01–0.5
N2 laser	337.1	3–6	0.1–0.6
XeCl excimer	308	20–30	0.5×10^3–10^3
KrF excimer	248	25–35	0.5×10^3–10^3
ArF excimer	193	8–15	8–15
Fiber laser-Ytterbium doped	1.03–1.08×10^3	5×10^{-5}–10^3	a
Fiber laser-Erbium doped	1.53–1.62×10^3	5×10^{-5}–10^3	a
Ti: sapphire	800	2×10^{-5}–2×10^{-4}	1–5

a Depends on both the pulse duration and the pulse repetition rate

Today Nd:YAG solid state lasers are the most useful laser kind in LIBS experimental set-up especially those with Q-switched key. It is possible to obtain narrow and intense laser pulses thanks to the appropriate optical technical features of the Q-switched Nd:YAG lasers. Nd-YAG lasers are usually pumped with Xe-arc flash lamps or diode pumped. But diode-pump lasers have high costs. A flash pumped actively Q-switched Nd : YAG laser is shown in figure 1.6 (Musazzi et al., 2014).

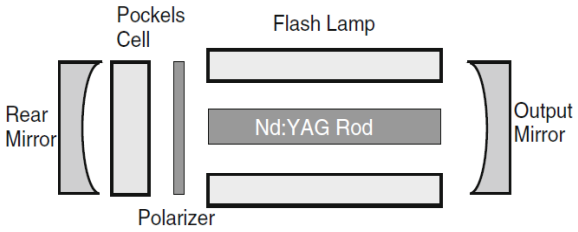

Figure 1.6. A flash pumped actively Q-switched Nd : YAG laser

(Musazzi et al., 2014).

In addition, thanks to the optical systems, the radiation is increased by focusing the laser beam on the sample in a small area. An ideal laser beam has a Gauss intensity profile and is expressed by the formula (Musazzi et al., 2014); $w_0 = \frac{f\lambda}{\prod D/2}$

where f is the lens focal length, λ is the wavelength of the laser radiation and D is the diameter of the unfocused beam onto the lens. It is possible to obtain high power density in the laser by using short-focus lenses at the focal point. Also, to obtain spatially resolved measurements short focal lenses can be used. Long-focus lenses are not kept close to the sample. The plasma stimulation procedure requires high energy when long focal lenses are used that provide a larger focal volume.

In addition, lenses are used to collect the emitted light and transmit it to the detector. The most important feature here is that the lenses must be optically permeable to transmit the emitted light to the detector.

In addition, there are highly reflective mirrors in the LIBS experiment set-up to direct the laser beam to optical devices. These mirrors should be selected according to the wavelength of the laser.

It is also used in optical fibers to perform remote LIBS experiments. However, in order for a high-energy laser beam not to damage the optical fiber, the plasma emission must be collected under suitable conditions (appropriate technology with optical fiber protection). With the recent optical fiber technologies, this problem has been solved to a large extent.

Wavelength selectors and optical detectors are used for spectral detection in LIBS experiments. The radiation emitted by the plasma is analyzed by this system

and the atomic species in the sample are determined. The ideal spectrometer-detector pair for detecting the emission of a wide spectral range from the vacuum ultraviolet to near-infrared has some important points. One of them is that the spectrometer has wide wavelength range and high spectral resolution. It must also have a wide dynamic range in its detector and give high quantum efficiency in its spectra. Another important point is that this system should be able to read and collect data in a short time.

There are different types of spectrographs. The most common of these are Czerny-Turner and echelle type of spectrograph. Figure 1.7 shows the Czerny-Turner spectrometer. The Czerny-Turner spectrometer is based on the use of a single dispersing element. In the Czerny-turner spectrometer, each spectral component leaves the grating propagating at a different angular direction. Eçhelle type spectrometers' resolution is higher than the Czerny-Turner spectrometers' resolution. The wavelength range of the Echelle type spectrometer is wide. (between 200nm and 1000nm) and it has high resolving power. The Echelle spectrometer has two dispersing elements, one of which is a grating and the other is a prism. Figure 1.8 shows the echell type spectrometer.

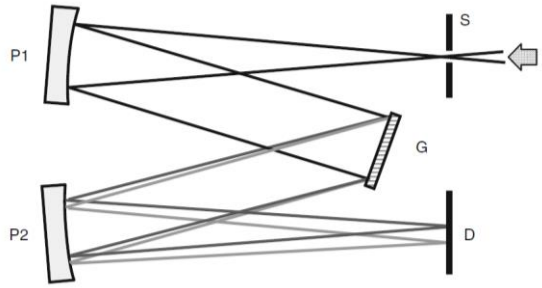

Figure 1.7. Schematic figure Czerny-Turner spectrometer

(Musazzi et al., 2014)

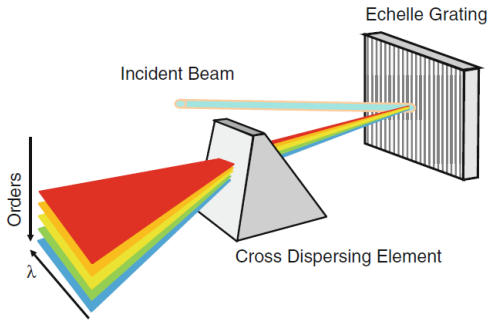

Figure 1.8. Schematic figure Echelle Spectrometer

(Musazzi et al., 2014)

Detectors are needed to convert the optical signal processed by the spectrograph into an electrical signal and analyze it through signal processor (such as a computer). Many different types of detectors are used. The most important ones are the photomultiplier tubes, the photodiodes, and an ICDD array detector, etc. The important point for LIBS analysis is its ability to perform multi-element and simultaneous measurements. Although the cost of the system is quite high, the use of an ICDD detector and echelle spectrograph together is one of the detector-spectrograph pairs that can meet this goal.

The detector consisting of image intensifier and optical connection with CCD is called ICDD detector. There are three main elements for an image intensifier; a photocathode, a microchannel plate (MCP), and a phosphor screen. Figure 1.9 shows the schematic viewing of the image intensifier (Musazzi et al., 2014). It has a simple working principle. Photons hitting the photo-cathode are converted into electrons. These electrons are accelerated towards MCP by applying control voltage. Incoming electrons are multiplied in the MCP. The electrons from the MCP crash into the phosphor screen and turn into photons. These photons are then transmitted to the CCD camera, which is the sensitive surface of the detector, with the help of fiber optics or lenses. At this point, in addition to the impact capacity of the incoming photoelectron number, the short shutter time (a few picoseconds) of the ICDD is also very important.

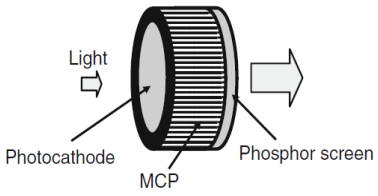

Figure 1.9.Schematic figure image intensifier

(Musazzi et al., 2014).

1.1.4 Advantages and Disadvantages of LIBS

LIBS technique has many advantages over other atomic emission techniques. If these advantages are listed as items;

- Versatile analysis of solids, liquids, and gases thanks to LIBS
- Since there is little or no sample preparation procedure, the LIBS technique has high efficiency, low contamination and is an easy method.
- Since a small amount of sample (~0.1 ug to 1mg) is sufficient when analyzing with LIBS technique, it is a practically non-destructive method.
- LIBS technique can be used for the analysis of very hard materials that are difficult to digest and dissolve, such as ceramics and superconductors.
- It can provide spatial resolution power in the range of 1-100 um for local analysis in micro-regions.
- Simultaneous multi-element analysis can be done.
- It has a direct detection feature when analyzing with aerosols (a solid or liquid particle in a gaseous medium).
- Since the ablation and excitation steps take place in one step, it has a simple and fast analysis capability.

Besides many advantages of the LIBS technique, there are some inadequacies ;

- Cost and system complexity may increase.
- It is difficult as a semi-quantitative analysis.

- Large interference effects such as potential interference of particle size are seen in the analysis of matrix interference and aerosols.
- The detection limit is not good especially for liquid analysis (low ppm range).
- Damage may be high when using high-energy laser pulses.
- Due to fluctuations in laser energy, shot to hot repeatability may vary, resulting in decreased sensitivity.

1.2. Liquid Analysis by LIBS

Although the LIBS technique can analyze all types of samples (solid, liquid, and gases), it is generally studied on solid samples. Liquid analysis with LIBS is more problematic experimentally than solids. These problems are splashing, bubble formation and shock wave formation, etc. As a result of these problems, together with the decrease in plasma emission, the results such as low signal intensity and high detection limits appear. Various techniques have been developed and used in liquid analysis with LIBS to overcome these problems. LIBS analysis with liquid can be carried out using different sample introduction techniques, for example, conversion from liquid to aerosol/gas phase (Aras et al.,2012) or liquid to solid conversion (Aguirre et al.,2013) techniques are used. It is also among other techniques used in double-shot lasers (Kumar et al.,2003). Apart from these, sampling techniques are used in other atomic spectroscopic techniques such as nebulizing methods (Kumar et al., 2003), electrospray ionization (Huang et al., 2004), and hydride generation (Ünal and Yalçın,2010) are methods used in liquid analysis with LIBS. Although these methods improve the detection limits in liquid analysis with LIBS, they eliminate the advantages of rapid and minimal sample preparation of laser-induced breakdown spectroscopy.

Bonding on different adsorbents (Alamelu et al.,2008 ; Lee et al.,2012), forming hydrogels (Guangmen et al., 2016), using nanoparticle (DeGiacomo et al., 2018) or nanofilm (Yang et al., 2017), and droplet dried on different substrates (Chen et al., 2008) are also used for the development of liquid analysis with LIBS. The use of nanoparticles in liquid analysis with LIBS has

an important place thanks to various physicochemical properties of metallic nanoparticles having large surface area, being mechanically strong, optically, and chemically active.

In the dry droplet LIBS technique, the sample is loaded on the appropriate substrate and dried. Then, high-energy laser pulses are sent onto this dried droplet, and analysis is done (Cahoon and Almirall, 2012; Aras and Yalçın, 2019). In this method, sample preparation is quite simple and fast.

All these liquid analyzes are also used fort he determination of heavy metals with LIBS.

1.3 . Heavy Metal Analysis by LIBS

Heavy metals analysis is important because of the enormous impact on human life and the environment. Among various analytical techniques for qualitative and quantitative analysis of heavy metals, Laser-Induced Breakdown Spectroscopy, LIBS, in the last decade, has become a preferred alternative due to its numerous advantages over the others. LIBS technique is a suitable technique for heavy metal analysis due to rapid sample preparation, small amount sample usage, simple technique, and applicable in any environment.

One of the LIBS studies in the literature is about the importance of food in human health. It is aimed to detect the toxic substances in foods with the LIBS technique (Sezer et al, 2017). In this study, many elements including heavy metals such as Pb and Cd are included.

Determination of heavy metals such as Cu, Pb, and Cr with nanoparticle and femtosecond LIBS is another example of literature work. It is concluded that the signal is low at the low laser energy level. They also observed that Ag nanoparticles amplify LIBS signals (Yang et al, 2017).

Looking at the recent studies, the analysis of heavy metals in the soil with LIBS has an important place. In a LIBS study (double pulse LIBS)

performed with a double pulse laser pulse, Cu, Ni, and Pb elements in the soil were determined (Chen et al., 2021).

The LIBS technique was used in a study based on the fact that the presence of excess Cd in cells would disrupt the enzyme activity. It has been proven that the measurement is made much faster than other methods thanks to the LIBS technique (Wang et al, 2021

CHAPTER 2

NANOPARTICLES ENHANCED LASER INDUCED BREAKDOWN SPECTROSCOPY (NELIBS)

2.1. General Information for NELIBS

Several articles in the literature indicate signal enhancements in the presence of metal nanoparticles, MNP, like Au and Ag, in dry-droplet analysis by LIBS and named as nanoparticle enhanced LIBS, NELIBS (DeGiacomo et al., 2018).

Signal enhancement in nanoparticle-enhanced LIBS, NELIBS (Bae D et al., 2015, DeGiacomo et al., 2016), is related to the changes in the ablation process. For most of the metal samples investigated, a significant decrease in the ablation threshold was detected. Nanoparticles can be used as an ideal thermal-insulation defect and they can change the optical properties of the target surface. Plasmons are formed on the surface of nanoparticles by sending a laser beam to the surface covered with nanoparticles. These surface plasmons and the laser's electromagnetic field enter into a strong interaction with each other, this event is called laser-matter interaction. Plasma formation can also be affected by macroscopic changes in the properties of the substrate surface and may have an impact on the optical emission. Optical changes in emission due to laser-matter interaction provide an increase in signal intensity. (Bae D et al., 2015, DeGiacomo et al., 2016, DeGiacomo et al., 2018).

2.2. Plasmonic Nanoparticles

The interaction between electromagnetic fields and free electrons in metals is called surface plasmon resonance (SPR). The free electrons found in metals are excited using the electrical components of light, thus collective oscillations occur. There are two types of collective oscillations as surface plasmon polariton (SPP)

that can spread on metal / dielectric interfaces and localized surface plasmon resonance (LSPR) that can spread around the nanoparticle /nanostructure. The common main event here is that the electromagnetic field is increased locally and localized at a deep sub-wavelength. For this reason, it has recently become one of the subjects with a wide range of uses in chemistry, biology, and energy. Plasmons have three main effects in nanoscience and nanotechnology, as they can achieve a great degree of freedom using the light of a certain frequency, achieve a huge increase under light intensity, and keep electromagnetic energy in volume/area /length at the deep wavelength (Liu et al., 2018).

Metal nanoparticles that absorb light and succeed in scattering light are plasmonic. They generally have diameters ranging in size from 10 to 150 nm. The most common are gold and silver nanoparticles. By changing the sizes, shapes, and surface coatings of nanoparticles, their colors can be displayed in the electromagnetic spectrum. The spherical gold nanoparticle solution has strong absorption and strong scattering. So it is located in the green region of the spectrum and is in the color of ruby red. Silver nanoparticle solutions are located in the blue region of the spectrum and their color is yellow. Figure 2.1 shows the surface plasmon resonance directed by the free electrons in the metal nanoparticles that driven them into oscillation with incoming light.

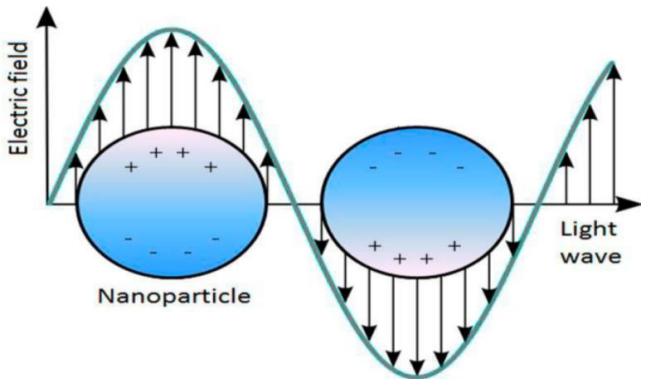

Figure 2.1. SPR scheme that occurs in oscillation with the combination of free conducting electrons and incoming light

(Unser et al.,2015)

The ability of specific wavelengths of light to push the transmission electrons in the metal to oscillate is a special spectral response to silver and gold nanoparticles. This property is called surface plasmon resonance (SPR). When plasmonic resonances are stimulated, provided that they are of the same size of particles, their absorption and scattering intensity can be up to 40 times higher than non-plasmonic ones. Therefore, their usage areas are very wide as mentioned before (Contra Costa College, 2013).

Particle size is one of the most important factors affecting nanoparticle absorption and scattering. If the wavelength of the light is larger than the metal nanoparticle, absorption becomes much larger than scattering.

2.2.1. Au- Ag Nanoparticles

The small size of the nanoparticles offers them unique properties. Since the surface area /volume ratios of nanoparticles are quite high, they are independent of their chemical components. Therefore, surface area properties play an important role in the solubility and stability of nanoparticles. However, the properties of gold in the nanoscale are different. Gold nanoparticles can be obtained in different shapes and sizes according to the method of production, so they can be used for different purposes. Their shape, size, and environment affect the interaction of gold nanoparticles with light. For example, if there is light near the nanoparticle, the electric field of the electromagnetic radiation and the free-floating electrons intreact, and a harmonic oscillation occurs between the light frequency and the resonant electrons. These oscillations are the surface plasmons mentioned earlier. As the particle size increases, the absorption wavelength increases, and the wavelength shifts to red and blue light is reflected. It is therefore blue or purple in solutions. The refractive index is among the factors affecting the optical properties of gold nanoparticles. When the refractive index increases towards the gold nanoparticle surface, the nanoparticle local surface plasmon resonance shifts towards the long wavelength. All these optical properties ensure that the use of gold nanoparticles is wide.

Silver nanoparticles range in size from 1 nm to 100 nm. They can be of different sizes and shapes by changing to the methods of production like gold nanoparticles production. The use of spherical silver nanoparticles is the most common. The extremely large surface area of the silver nanoparticles allows them to be used in ligand coordination. If silver nanoparticles interact with a certain wavelength of light, just like gold nanoparticles, together with the electromagnetic field in the light, free electrons in the environment create a harmonic oscillation. In this event, which is called surface plasmon resonance, the amplitude of oscillation is at a maximum in a certain frequency. Particle size, shape, and refractive index affect the absorption and scattering properties of silver nanoparticles. Large nanoparticles have less power to absorb light but scatter more than small nanoparticles and give a peak at longer wavelengths. Silver nanoparticles have advantages such as high extinction coefficient, sharp extinction bands, high area enhancements.

2.3. Literature Works

2.3.1 Ag Nanoparticles Literature Works

Since nanoparticles are known to interact strongly with light, one of the studies conducted with the belief that there will be an increase in signal in surface-enhanced Raman spectroscopy belongs to Tamaru et al (2002). Considering the results of the study, it was observed that there is a strong correlation between resonance frequencies and shape anisotropy.

In a study by Huang and Xu, twelve separate Ag Np syntheses with an absorption spectrum between 393 and 738 nm and different colors, sizes, and shapes were performed (2010). In this study, the relationship between the size and shape of the synthesized Ag nanoparticles and the scattering localized surface plasmon resonance (LSPR) spectra were investigated. Synthesized Ag nanoparticle colloids are in the form of spherical, rod, triangle, and cookie. When looking at LSPR spectra, nanoparticle colors showing Imax are blue (476±5 nm), green (533±12nm), yellow (611±23), and red (711±40). Looking at the results, it has been

observed that it is possible to adjust the optical properties of Ag nanoparticles in the ensemble by using single nanoparticle sizes and shapes. In figure 2.2, the photograph of Ag Nanoparticle colloid solutions synthesized is shown in A part, and B is the absorbance of UV-Vis absorption spectra of these nanoparticles.

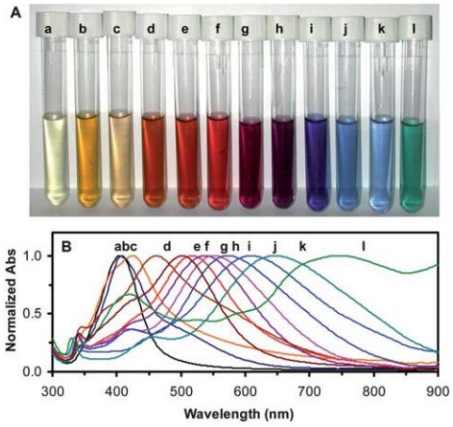

Figure 2.2. a) Colloidal solutions of synthesized AgNPs b) UV-VIS absorption spectra of synthesized AgNPs

(Huang and Xu, 2010).

In another study, using the new photochemical synthesis method, Ag nanoparticles in different sizes and shapes and accordingly in different colors were produced (Stamplecoskie and Scaiano,2010). In this synthesis method, LEDs are used as photochemical sources. Figure 2.3 shows the colors and absorbance wavelength of the synthesized Ag nanoparticles.

Figure 2.3. Colors and absorbance wavelengths of synthesized AgNPs (Stamplecoskie and Scaiano,2010)

Nanoparticles have unique properties thanks to their differences in size and shape, stabilizers, interactions with the environment, and different preparation methods. Thanks to the new synthesis methods developed recently, it has been made possible to synthesize triangularly, 5 or 6 diagonal, disk-shaped, and three-dimensional (cubic, pyramid) nanoparticles instead of spherical shapes. The reaction rates of different nanoparticles are also different (Khodashenas and RezaGhorbani, 2019).

When plasmons interact with metal nanoparticles with excitons or semiconductor quantum dots, plexcitons (plasmon-exciton polariton) occur. These plexcitons are produced using wet chemistry methods or using different lithographic techniques. In the study carried out by Balcı et al.,(2019) Silver nanoparticles with nanoprism shapes were synthesized by using seed-mediated synthesis based on very high Rabi-splitting energies. These synthesized silver nanoprisms were transformed into silver nanoparticles in nanodisks under high-temperature conditions. Finally, J-aggregated dyes combine with nanodisk-shaped silver nanoparticles to form plexcitonic silver nanoparticles. According to the results of this study, it is thought that these plexcitonic nanoparticles, which have high Rabi-splitting energy and very good stability under room conditions, can have a wide range of uses. Figure 2.4 shows the transformation of plasmonic spherical silver nanoparticles into plexcitonic nanodisk silver nanoparticles with shape changes.

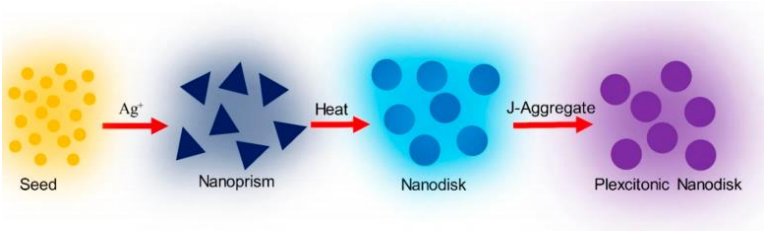

Figure 2.4. Shape evolution of plasmonic silver nanoparticles

(Balcı et al.,2019)

2.3.2. NELIBS Literature Works

NELIBS are among the topics whose work has increased recently. One of these studies is an analysis of metal samples made by De Giacomo et al (2013). In this study, a 1-2 times increase in LIBS signals of metal solid samples was observed using silver nanoparticles. When using Ag nanoparticles up to 10 nm diameter and 1 order size concentration, it was observed that the analyzed sample's emission signal was not affected much, and therefore the NELIBS method was found to be effective for the analysis of metals. One of the most proven points in this study is that there is no experimental setup difference between LIBS and NELIBS. Therefore, the fast, easy and practical feature of the LIBS technique is valid for NELIBS studies. The biggest reason for the increase of the signal intensity is that the ablation threshold decreases with NELIBS. On the other hand, there is no difference between LIBS and NELIBS when the plasma parameters consisting of temperature and electron number density are examined. Summary of this study Ag nanoparticles has been successful in providing a 1-2 times increase in the chemical analysis of solid metal samples without the need for a different LIBS experimental set-up.

Another study by El Sherbini and Parigger (2015), they have investigated wavelength dependency and threshold measurements for nanoparticle-enhanced laser-induced breakdown spectroscopy. For this study, zinc monoxide nanoparticle was used. Studies were carried out with Nd: YAG laser device at 1064, 532, and 355 nm. Looking at the results of this article, the enhancement is related to the decrease in laser fluence threshold value. One of the reasons for this decrease in threshold value is the reduction of the bulk thermal conduction length in the target material to the nanoparticle size in the nanomaterial. In addition, as the laser wavelength increases, the laser fluence threshold value for bulk materials decreases. Another conclusion of the article is that in order for plasma production to occur, multiple photon ionization and electron pulse ionization must be combined.

Another nanoparticle application of LIBS was performed by De Giacomo et al. in 2016. In this study, the analysis of the effect of nanoparticles on laser ablation and plasma emission was performed. In this study, silver, gold, platinum, and copper nanoparticles which are metallic were used. As in the previous study, an

increase of 1-2 times was observed in the signal intensity. In this analysis, after the nanoparticle colloidal solution was placed on the sample as a micro drop and dried, the analysis was performed. In addition, to analyze the effect of nanoparticle size on the signal, analyzes were made with silver nanoparticles of 20 nm and 10 nm in size, thus characterizing the nanoparticles in terms of their size and concentration. Considering the results, it is seen that the emission signal is high as the particle size increases. Due to the low thermal conductivity of nanoparticles, ablation of nanoparticles occurs when they are dropped on non-conductive samples. At this point, the improvement in the spectra is due to the presence of multiple firing points and the instantaneous escape of electrons during the emission period when the nanoparticles are dropped onto the conductive sample.

It is important that the determination of the elemental composition of micro drops at sub-ppm level. De Giacomo et al. (2016) investigated the evaluation of nanoparticle enhanced laser-induced breakdown spectroscopy for the determination of elemental analysis of micro drops of 1 uL volume of liquid solutions, in single-shot mode. For this study, Teflon, glass, and silicon were used as a substrate, while gold nanoparticle was used as a nanoparticle. It has been observed that gold nanoparticles show an improvement in the analyte signal. It has been observed that there are three main reasons for this improvement. The first and the most basic of these is that the electromagnetic field in the laser and the surface plasmon of the nanoparticle combine to improve the field. Finally, the plasma density is increased by the ablation of nanoparticles. In addition, studies have been performed on human serum solutions and proteins contaminated with metal ions. In this area, a different healing effect of the nanoparticle has been observed. Plasma is better stimulated if the analyte consists of atoms with high ionization energy. The most important event at this point is the possibility of metal analysis at micro levels in human serums.

In another study by De Giacomo et al. (2016) discusses the effect of nanoparticles on metal samples to increase the emission signal with laser-induced breakdown spectroscopy. Both the basic aspects and the application aspects of placing nanoparticles on the sample are discussed. Gold and silver nanoparticles with a volume of 1 microliter were used. Experiments were carried out in three different typologies: metals, glass, and liquid solutions. As in previous studies, the reason that the nanoparticle improves the emission signal intensity is that the

electromagnetic field in the laser combines with the surface plasmon of the nanoparticle and decreases ablation threshold energy, thereby increasing ablation efficiency. Another important study is that the injection method was used. Atoms and ions in the nanoparticle have been ionized and increased the plasma density, thus allowing a small amount of sample to be analyzed by NELIBS. Working with metal analytes provides the most effective results when working with NELIBS because nanoparticles produce a good electrical interaction with metals. On transparent surfaces such as glass, working with normal LIBS is difficult due to the low repeatability resulting from laser impact damage. At this point, it was thought that this difficulty could be overcome by putting nanoparticles on the surface. Looking at the results of the article, 1-2 times enhancement was observed in the signals. When performing LIBS analysis with liquids, using a small amount of liquid makes the analysis difficult. Since the sensitivity of LIBS will increase when the nanoparticle is used in the study, it has been proven that analysis with a small amount of liquid sample is possible.

Another interesting study performed by Zhao (2019) was about harmful chemicals in fruit and vegetables. The detection of chemicals in fruits and vegetables is vital for human health. With normal LIBS, analysis is difficult in terms of the determination limit. In this study, trace amounts of pesticides and heavy metals can be determined using metal nanoparticles. A silver metal nanoparticle of 80 nm size was used as nanoparticle. In addition, emission signals have been proven to be more intense and there has been a 2-times improvement in emission signals. As with other nanoparticle studies, the improvement in the emission signal has been linked to two reasons. The first is to increase the electron density by using the silver nanoparticle and the second is to decrease the ablation threshold energy.

Another literature study is about synthesizing nanoparticles using the LIBS technique (Quayyum et al., 2019). In this study, silver and gold nanoparticles were synthesized for use in NELIBS. Silver and gold discs in pure water were used using the laser ablation method. It was observed that the size of the silver nanoparticles was larger than the gold nanoparticle dimensions. For NELIBS studies, soda-lime glass and copper samples were used as samples. An enhancement in the signal intensity was observed in both nanoparticles. It was predicted that this was due to

the combination of the laser electromagnetic field and the nanoparticle surface plasmon. The enhancement in the Signal intensity was higher when gold nanoparticles were used. The reason for this is that the size of the gold nanoparticle is smaller than that of the silver nanoparticle.

One interesting biological application of LIBS in the literature that belongs to Dell'Aglio (2019) is about the application of gold nanoparticles embedded in the amyloid fibrils by NELIBS. In this study, amyloid fibrils were covered with gold nanoparticles and were used in the metal analysis by laser-induced breakdown spectroscopy. Normally, proteins extinguish the plasma, making analysis difficult. However, thanks to the use of gold nanoparticles, the problem of plasma extinction is largely eliminated. Gold nanoparticles increased the atomization efficiency of the organic sample. The metal analytes are bonded with amyloid fibrils and the detection of metals takes place. Thanks to the golden nanoparticles, it was possible to detect Cr, Pb, Tl, and Cd metal elements at the level of ppm (mg/kg) in proteins.

In another study by Kiris et al. (2019), they have compared the efficiency of the LIBS signal intensity when used Ag-Cu and Ni-C NPs in the visible and UV ranges. Ag-Cu and Ni-C nanoparticles were synthesized by laser ablation and spark discharge method. While analyzing with laser-induced breakdown spectroscopy, nanoparticles were deposited on aluminum foil and signal increases were observed. Signal increases are between 2-20 times and Ag-Cu nanoparticles were more effective in signal increases.

Another NELIBS study was performed by Palasti et al. (2020) using Ag nanoparticles on indium-tin-oxide. Indium-tin oxide has been termed modified surface-enhanced Raman scattering substrates. Ag Nanoparticles have been used in different sizes. Liquid states of Mn, Zn, and Cr elements were analyzed by the spraying method. A 3-times increase was observed in the signal.

In the NELIBS study with Ag nanoparticles with nanosphere, nanocubes, and nanowires shape, the effect of nanoparticle shape on LIBS signal was investigated (Abdelhamid et al., 2020). When looking at the results, it has been observed that silver nanoparticles in nanocube and nanowire form have a stronger absorption mechanism than silver nanoparticles in nanospherical shape, so they are more effective in LIBS signal intensity. The reason why the signal intensity is highest in

nanowires is that the photocatalytic activity is higher depending on the shape. On the other hand, Ag nanoparticles in the form of nanocube are said to have an extra boosting effect on the line intensities of their corner and surface sections.

Looking at a recent NELIBS study, the effect of the Ti element on the LIBS signal intensity of Au nanoparticles with different sizes (10, 40, 60, 100 nm) was investigated (Salajkova et al., 2021). One of the important points when working with nanoparticles of different sizes is the concentration of nanoparticles deposited on the surface, or the distance between nanoparticles. If the optimum distance is provided between the laser electromagnetic field and the nanoparticle surface plasmons, the nanoparticle size does not matter. Therefore, nanoparticle concentration is one of the most important parameters when working with NELIBS. In addition, it has been stated that plasma parameters such as temperature and electron density are not related to the electromagnetic field, so they are not very different in LIBS and NELIBS studies.

2.3.3. Motivation

In this thesis the effect of silver nanoparticles with different shapes, sizes and spectral properties on the LIBS signal of Lead and Chromiumin a liquid sample dried on the substrate was investigated. The use of AgNPs of different sizes and shapes with LIBS has emerged because the electromagnetic field of the laser forming the plasma and the free electrons in the environment affect the LIBS signal intensity. In addition, the signal is expected to increase as the plasma becomes brighter and stronger with the nanoparticle effect.

CHAPTER 3

EXPERIMENTAL

3.1. LIBS Experimental Set-up

In this study, the LIBS experimental set-up was optimized for the determination of lead and chromium in the prescence of silver nanoparticles having different maximum absorption wavelength and shapes. LIBS parameters such as laser energy, detector gate time, and delay time were optimized with standadr solutions of lead and chromium dried on silicon nitride, which was used as substrate. Based on the literature, firstly, the change in signal intensity was observed in the determination of Pb in the prescence of spherical silver nanoparticles. Then, the signal intensity improvement of the prism and disc-shaped silver nanoparticles with different spectral properties was studied.

3.1.1 Laser and Optic Materials

An experimental LIBS set-up schematic diagram and the actual view are shown in Fig. 3.1. A Q-switched Nd : YAG laser source (Quanta-Ray Lab-170, Spectra- Physics, California- USA) with 10 ns duration time has been operated at its second harmonic wavelength, 532 nm. The laser beam is directed on the target by reflective mirrors (1'' OD, coated, 532 nm reflective, New Focus, Darmstadt-Germany) and is focused onto the sample surface by a 17.5 cm focal length plano-convex lens placed at a position 15.5 cm away from the sample. Laser pulse energy is measured by a power meter (PE50BB-DIF-V2, Nova II, Ophir).

a) b)

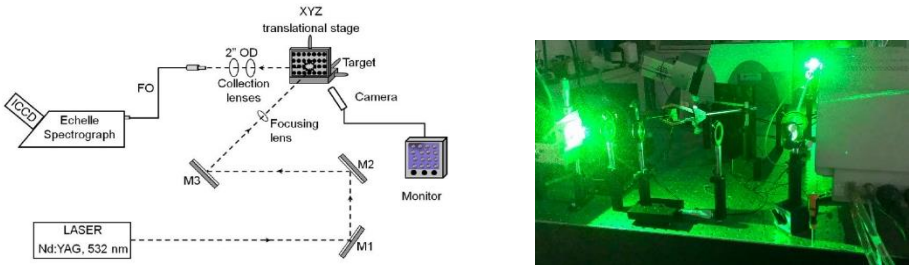

Figure 3.1. a) Schematic diagram of LIBS experimental set-up

(Aras and Yalcin, 2019) b) actual view of the LIBS experimental set-up

The analysis was carried out by placing the silicon nitride wafer in the place called the XYZ translation stage (New Focus, Darmstadt-Germany). Thanks to the XYZ translation stage, analysis of more than one dry droplet was possible. A silicon nitride substrate containing Pb and Cr standard solution and nanoparticle was placed on the XYZ translational stage. The plasma formed as a result of the sent laser beam is transmitted to the fiber optic cable (Ocean Optics,P600-2UV-VIS,600 μm diameter) by means of two plano convex lenses with focal lengths of 5 and 10 cm. The task of the fiber optic cable here is to transmit the plasma emission to the echelle spectrograph.

3.1.2. Detection System

In this study, the Echelle spectrograph (Mechelle 5000, Andor Inc., f/7) equipped with the charged coupled device (ICCD) (iStar DH734, Andor Inc.). The spectral range of the Echelle spectrograph lies between 200 and 850 nm, and at 400 nm has a resolution of 0.08 nm. The wavelength calibration of the spectra was carried out with the help of the Hg-Ag calibration lamp. ICDD detector system was to monitor. Optimization studies were carried out achieve highest signals for Pb(I) at 405.8 nm and Cr(I) at 428.9 nm. These optimization parameters are detector gate time, delay time, and laser energy.

3.2. Substrates and Chemicals

3.2.1 Silicon Wafer Substrate

One type of silicon wafer-based substrates: 300 nm silicon nitride layer on c-Silicon wafer substrate (Si_3N_4+Si) was used. Figure 3.2 shows the droplets of the Pb solution on a Si_3N_4 wafer.

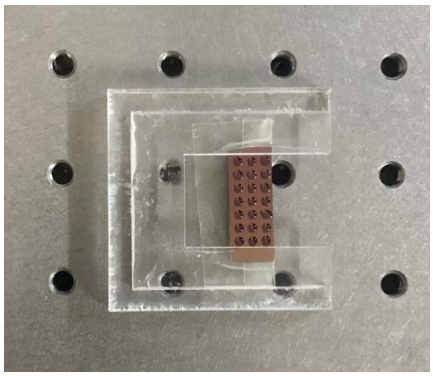

Figure 3.2. Droplets on Si_3N_4 wafer

3.2.2 Chemicals

Various chemical aqueous solutions have been used for heavy metals optimization studies, analysis with nanoparticles, and calibration graphics. High Purity Standards, LEAD 1000 ppm in 2% HCl standard aqueous solution was used for optimization studies and calibration plots of the Pb element. For the usability of the method in the matrix, the High Purity Standards 7 Component Primary Drinking Water Metals in 2% HNO_3 + Tr HF Solution A-100 standard aqueous solution was used as a reference water sample.

High Purity Standards (HPS), CHROMIUM 1000 ppm in 2% HNO_3 aqueous standard solution was used for optimization studies and calibration plots of the Cr element. For the usability of the method in the matrix, the High Purity Standards 7 Component Primary Drinking Water Metals in 2% HNO_3 + Tr HF Solution A-100 standard aqueous solution was used as a reference water sample.

In the determination of Pb, the accuracy of the method was tested by spiking drinking water purchased from local market.

For spiking experiments for Cr heavy metal, experiments were carried out with SLRS-4 Riverine water Eau fluvial water sample.

3.3. Ag Nanoparticle Synthesis

The synthesis of the spherical, prism and disc-shaped nanoparticles used in this study was carried out by the Izmir Institute of Technology, Department of Photonics, Sinan Balcı Laboratory.

The spherical-shaped nanoparticles were then synthesized in an aqueous environment to be used as silver seeds in the synthesis of prismatic nanoparticles. For this synthesis, the first 5 mL of 2.5 mM trisodium citrate solution and 0.25 mL of 500 mg/L poly (sodium 4-styrene sulfonate) (PSS) were mixed. Then 0.3 mL of a 10 mM $NaBH_4$ solution, a strong reducing agent, was added. Then, 5 mL of 0.5 mM $AgNO_3$ solution was added dropwise and stirring was carried out during this time. After approximately 30 minutes, a yellow-colored silver colloidal solution was obtained.

Silver seeds were used for the synthesis of prism-shaped nanoparticles. Millipore water, 75 uL of 10 mM ascorbic acid, a weak reducing agent, and 60 uL of synthesized silver seed were mixed. Then 0.5 mM $AgNO_3$ solution was added dropwise to this mixture and stirring was performed at this stage. During this process, the color of the colloidal solution changes from yellow to red, then from red to blue, according to the resonance wavelength according to the amount of $AgNO_3$ solution added. For example, if 3 mL of $AgNO_3$ solution is added dropwise, a blue-toned silver-nanoparticle solution with maximum absorption wavelength of 700 nm is obtained silver nanoparticle. At this step, 0.5 mL of 25 mM trisodium citrate solution was added to ensure stabilization.

To obtain silver nanoparticles in the form of a disc, the prism-shaped nanoparticles were heated in an oil bath at 95°C by stirring.

3.4. Uv-Vis Spectral Analysis of AgNPs

Absorbance measurements of silver nanoparticles were made with a spectrometer (USB4000, Ocean Optics), which has a deuterium-tungsten halogen light source (DH2000-BAL, Ocean Optics) and is connected to the fiber(727-733-2447).

3.5. Dynamic Light Scattering Measurements

The size measurements of the synthesized silver nanoparticles with spherical, prism and disk shapes were carried out by Dynamic Light Scattering (DLS) device. (Zetasizer, Malvern) . The device performs a measurement based on the refractive index. Water was used as the dispersant solvent. For measurement, 1 mL of deionized water and 40 microliters of AgNP were added to the cuvette. If the concentration is too much, the measurement cannot be made, so dilution is performed. To perform the measurement, the measurement type has been selected as size in the Software section. As a sample, Ag was entered and the measurements were made by setting the temperature to 25°C degrees.

3.6. STEM Analysis

The image and size measurements of the synthesized some silver nanoparticles were carried out by STEM analysis in Izmir Institute of Technology Center for Materials Research. Grids were used for STEM analysis. Care was taken to ensure that the sample was dry so that the analysis could be carried out. The surface distribution of nanoparticles could not be observed due to the fact that the substrate was grid rather than silicon wafer during the analysis.

3.7. Dried-Droplet Analysis

In this study, the dry droplet technique was used both optimization studies and nanoparticle studies. This technique includes three steps; loading, drying, analyzing. Calibration standards for Pb element were prepared from its stock solutions by serial dilutions with distilled water. 500 nanoliter droplets of analyte solutions (Pb) loaded on the silicon-wafer substrate, are analyzed with energetic laser pulses after drying at room temperature. Calibration standards for Cr element were prepared from its stock solutions (High Purity Standards, CHROMIUM 1000 ppm) by serial dilutions with distilled water. 500 nanoliter droplets of analyte solutions (Cr) loaded on the silicon-wafer substrate, are analyzed with energetic laser pulses after drying at room temperature.

When studying with nanoparticles, 500 nanoliters droplets of NP's were loaded on the silicon-wafer substrate after drying 500 nanoliters of analyte solution was loaded on the same spot on NPs residues, in the form of thin-film layer and analyzed with energetic laser pulses. Figure 3.3 shows the SEM image of the dried droplet silicon nitride wafer and the picture and SEM image of the laser pulsed silicon nitride layer.

a) b) c)

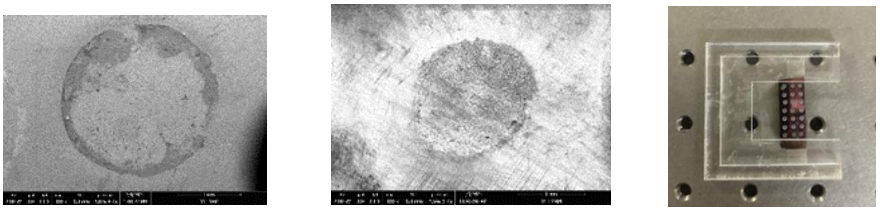

Figure 3.3 a) SEM representation of dried droplet Si_3N_4 wafer c)SEM representation of laser-ablated Si_3N_4 wafer b) Pictorial of laser-ablated Si_3N_4 wafer

CHAPTER 4

RESULT AND DISCUSSION

In this thesis, the LIBS system was optimized to investigate the effect of AgNPs, which have maximum absorbance at different wavelengths, on signal intensity in the determination of Pb with LIBS. Then, analyzes were made on the Cr element with the silver nanoparticle in the absorbance where the highest signals were obtained.

4.1. Optimization of experimental LIBS parameters

Before starting the NELIBS studies, optimization studies were carried out to determine the detector timing parameters and laser energy of Pb (I) heavy metal. As a result of the determined optimum conditions, NELIBS studies were continued using AgNP. The LIBS spectrum for the lead element is included in Figure 4.1.

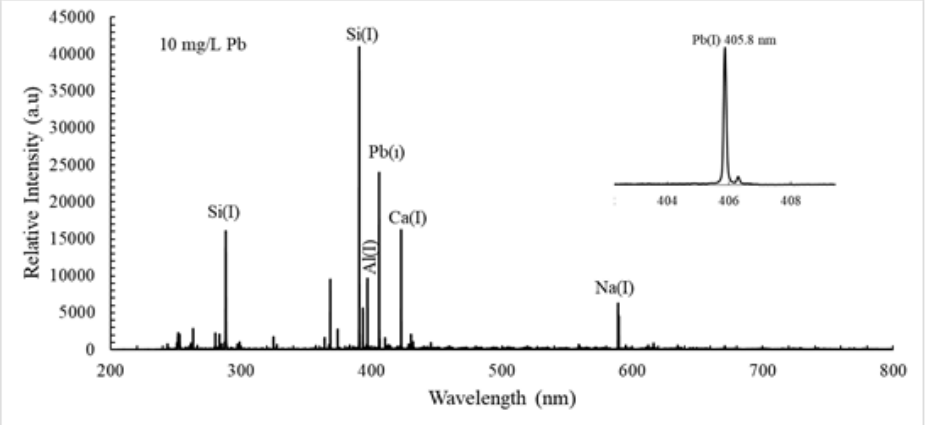

Figure 4.1. Typical LIBS spectrum of Pb(I) 405.8 nm Laser pulse energy 130 mj, delay time 2 μs, gate width 500 μs, detector gain 100, 4 single shot accumulation,10 ppm Pb.

According to the spectrum in Figure 4.1, the Pb element has a high signal intensity at a wavelength of 405.8 nm. The transition at this wavelength is also seen

as a Grotrian diagram in figure 4.2. Optimization studies were made based on this wavelength.

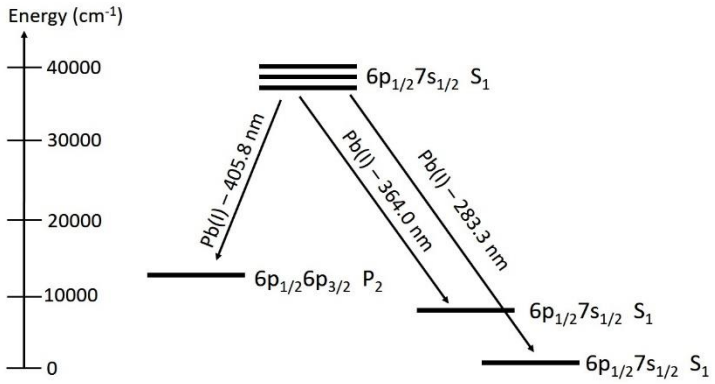

Figure 4.2. Grotrian Diagram for Pb at 405.8 nm emission

It is seen that the emission wavelength of 405.8 nm comes from a triplet energy level.

4.1.1. Delay time

To get high efficiency from spectra, low levels of backgrounds should be obtained against intense signals from plasma. Time resolution parameters are of great importance for this. One of these time resolution parameters is called detector delay time. In very early times (eg 300 ns and below) the detector sees the laser beam. This is both harmful to the detector and undesirable data in the spectrum. In order to determine the optimum delay time of the Pb heavy metal, studies were carried out at different time intervals by keeping all other conditions (such as detector gate time: 500μs, laser energy: 130 mj) constant. Figure 4.3 shows the signal intensity change of Pb (I) heavy metal at 405.78 nm according to the detector delay time.

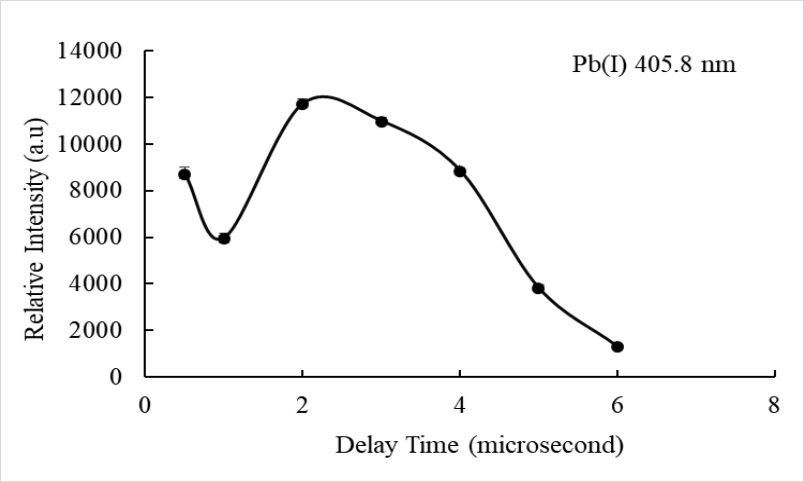

Figure 4.3. Optimization studies of detector delay time for Pb(I) at 405.8 nm. Laser pulse energy 130 mj, gate width 500 μs, detector gain 100, 4 single shot accumulation,10 ppm Pb.

4.1.2. Gate Time

Another important time resolution parameter is called the detector gate time. Similar to the operations in the detector delay time, this time the detector delay time (2μs) and laser energy (130 mj) were kept constant and studies were carried out with different time intervals, and as a result, the optimum detector passage interval for lead was determined. Figure 4.4 shows the signal intensity change of Pb (I) heavy metal at 405.78 nm according to the detector gate time.

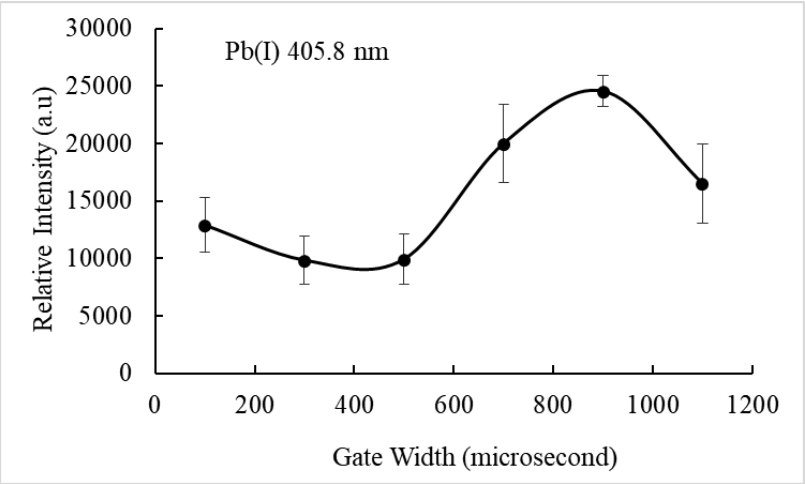

Figure 4.4. Optimization experimental studies of detector gate time for Pb(I) at 405.8 nm. Laser pulse energy 130 mj, delay time 2 μs, detector gain 100, 4 single shot accumulation, 10 ppm Pb.

4.1.3. Laser Energy

Laser energy is among the most important parameters for plasma formation in LIBS analysis. The temperature of the plasma formed, the ablation mechanism and the magnitude of the ionization procedure depends on the laser pulse energy. Low laser energies cause low plasma density and therefore low signal intensity. High laser energy, on the other hand, causes a lot of damage to the analyzed sample and also leads to non-stoichiometric ablation. This is called plasma shielding. Also, very high energies can lead to self-absorption. This is a factor affecting plasma opacity. Plasma is optically thin. If self-absorption is observed, this optical fineness is widened and the element's emission peaks shift. For all these reasons, optimum laser energy is determined for emission signal intensities with high S / N (signal/noise) in LIBS analysis. Studies have been carried out at different laser energy intensities to determine the optimum laser energy for Pb determination. Figure 4.5 shows the Pb (I) signal intensities against different energy intensities.

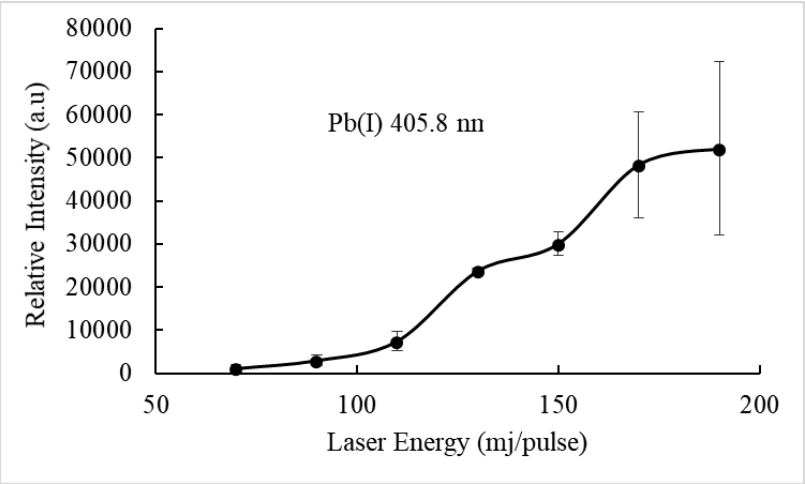

Figure 4.5. Optimization experimental studies of laser energy for Pb(I) at 405.8 nm. Delay time 2 μs, detector gate time; 900 μs, detector gain 100, 4 single shot accumulation, 10 ppm Pb.

As a result of optimization studies, for Pb element, the optimized delay time, the gate time and the laser pulse energy was determined as 2 μs, 900 μs, and 130 mj, respectively. Also using 4 single shots in total was found to be the optimum value.

A typical Boltzman plot from Na(I) lines obtained at optimized conditions can be seen in figure 4.6. The reason why Pb peaks are not used when calculating plasma temperature is due to the fact that they have a small number of severe peaks. From the slope of this graph, the plasma temperature under optimized conditions was found to be 11815 K. Since a typical LIBS plasma temperature is between 10000K and 20000K, the temperature value found is between acceptable values. The reason for this plasma temperature, which is not very high, is due to the fact that the substrate is silicon nitride. The silicon nitride layer absorbs the laser light very well and cools the plasma itself. This good absorption mechanism enables it to transfer energy transfer to the sample very efficiently and contributes to high signal intensities.

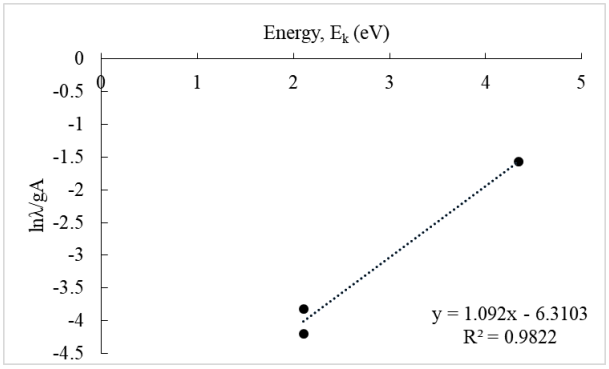

Figure 4.6. Typical Boltzman plot that used for temperature calculation obtained from Na(I) lines under optimized conditions.

McWhirter criterion was used to control the local thermal equilibrium (LTE) value. LTE requires the minimum electron number density which can be determined by the equation $N_e \geq 1.6x10^{12}\, x\, T_e^{1/2}\, x\, (\Delta E)^3$ (Hahn and Omenetto, 2010). T(K) represents the electron temperature and ΔE (eV) is the difference in energy between the two states. The energy difference between upper and lower levels for lead line at 405.8 nm is 3.05 eV. Electron density is $4.93x10^{15}$. This value close to LTE value.

4.2. Ag Nanoparticle Synthesis

Silver nanoparticles with spherical, disc, and prism shapes were synthesized at the Sinan Balcı Laboratory of Izmir Institute of Technology. For the synthesis of silver nanoparticles with prism and disc shape, silver nanoparticle with a spherical shape was synthesized first. Figure 4.7 shows the synthesized spherical silver nanoparticle. Its color is close to yellow.

Figure 4.7. Synthesized spherical (seed) Ag Nanoparticle

After the seed silver nanoparticle synthesis, silver nanoparticle synthesis with prism shape was performed. Depending on the amount of $AgNO_3$ added, the color of the prism-shaped nanoparticles synthesized varies between pink-purple and blue. Figure 4.8 shows the synthesized prism-shaped silver nanoparticles.

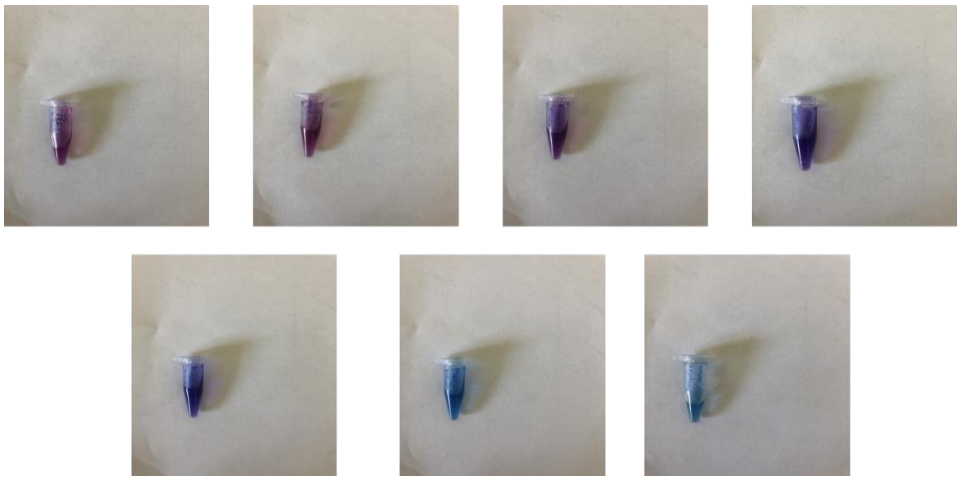

Figure 4.8. Synthesized prism-Ag Nanoparticle

Prism-shaped silver nanoparticles were heated in an oil bath and synthesis of silver nanoparticles with disc shape was made. Figure 4.9 shows the synthesized disc-shaped silver nanoparticles. Similar to the prism-shaped silver nanoparticles, the disc-shaped silver nanoparticles show a distribution between pink-violet-blue colors in proportion to their absorbance wavelengths.

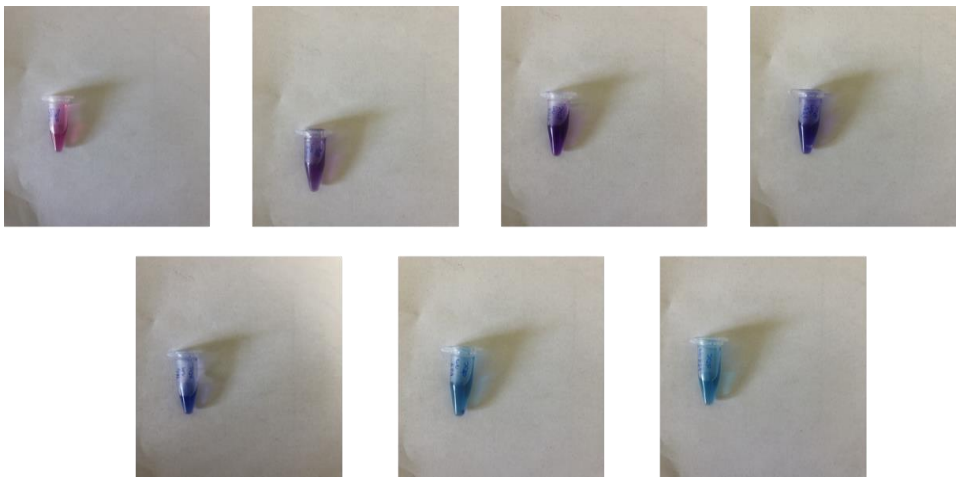

Figure 4.9. Synthesized disc-Ag Nanoparticle

Concentration measurements of nanoparticles were found by centrifugation. The nanoparticle solutions added at the same rate to the vials of the same capacity were precipitated by centrifugation and their masses were measured. The concentration of all silver nanoparticles synthesized is 0.02 mg / mL.

4.3. UV-Vis Absorption Spectra of AgNPs

UV-VIS measurements of the synthesized silver nanoparticles were carried out with a spectrometer equipped with a deuterium and tungsten halogen lamp source. The UV-VIS absorption peaks of the synthesized silver nanoparticles vary between 390 nm and 770 nm depending on their size, shape and distribution. Synthesized nanoparticles have an electromagnetic field frequency of their own. They make a strong absorption with the resonance that occurs between these electromagnetic field frequencies and electron movements. Therefore, each one has its color source at different wavelengths. In addition, the plasmon resonances of the prism-shaped silver nanoparticles can be adjusted in the visible spectrum by adjusting the amounts of the seed, namely the spherical silver nanoparticles in the colloid. UV-Vis spectra of spherical, disc, and prism-shaped Ag NP are given in Fig. 4.10 (a-c), respectively. Looking at the spectra, a spherical silver nanoparticle with an absorbance wavelength of 394 nm was obtained. It has a color close to yellow in the visible region. When looking at the absorbance of silver nanoparticles with prism shape; It is seen that they have maximum absorbance wavelengths at 535 nm, 540 nm, 548 nm, 578 nm, 596 nm, 688 nm, 761 nm. As seen in the absorbance wavelengths of the silver nanoparticles in the form of a disc; 515 nm, 524 nm, 544 nm, 555 nm, 564 nm, 637 nm 651 nm. Looking at the spectra, a gradual blue shift resonance is observed in the plasma of the disc-shaped silver nanoparticles. In addition, the resonance frequencies of the plasmonic disc silver nanoparticles in the visible spectrum can be adjusted by the temperature control of the nano prisms silver nanoparticles.

(a)

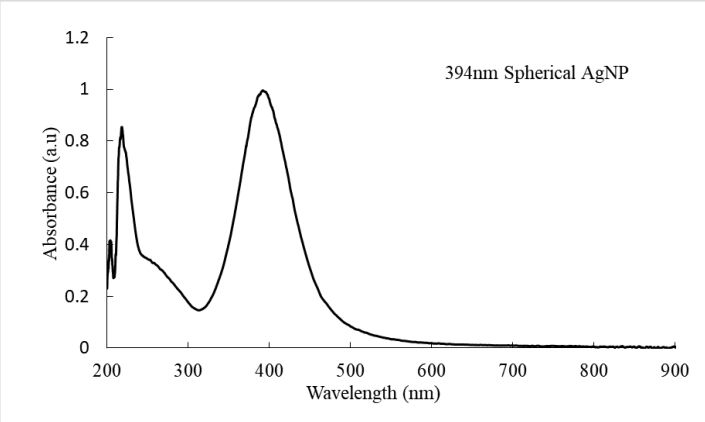

(b)

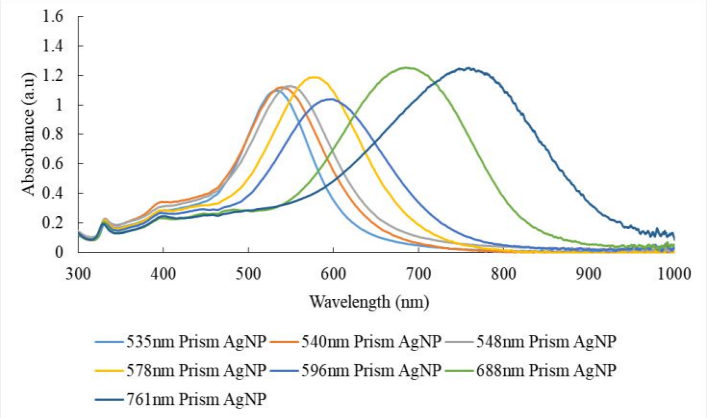

(c)

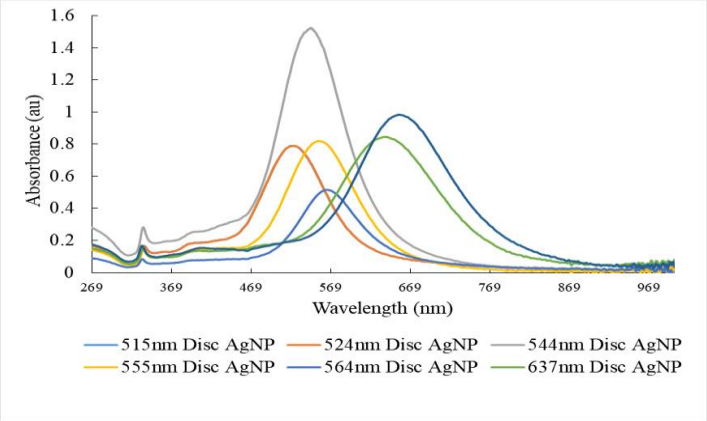

Figure 4.10. a) UV-Vis spectra for synthesized seed silver nanoparticles. b) UV-Vis spectra for synthesized prism silver nanoparticles. c) UV-Vis spectra for synthesized disc silver nanoparticles

4.4. Dynamic Light Scattering Measurement

The size measurements of the synthesized silver nanoparticles were performed by Dynamic Light Scattering (DLS) device. An example of size measurements of the prism and disc-shaped nanoparticles are given in Figure 4.11. The first peak on the graph shows the thickness of the silver nanoparticle and the second peak shows the size of the silver nanoparticle. Peak separation is difficult for thickness sizes because they are very close to each other in size.

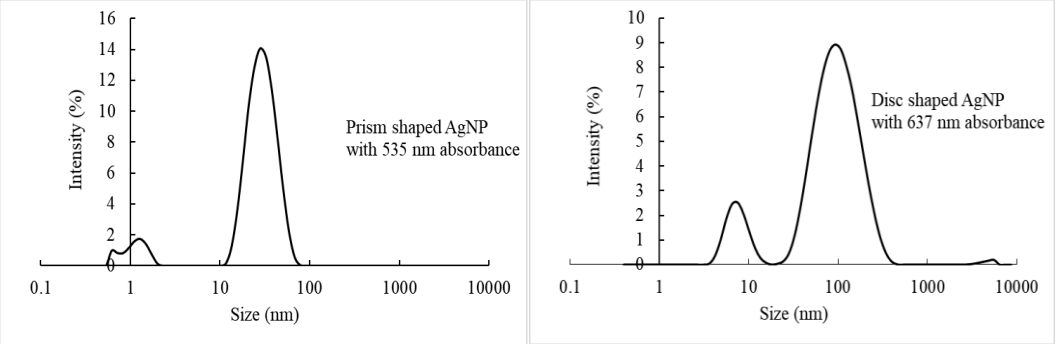

Figure 4.11. DLS graphs Ag nanoparticles

Table 4.1 contains the size information for differently shaped silver nanoparticles obtained from DLS measurements.

Table 4.1. Size of the prism and disc-shaped AgNPs.

Prism AgNPs absorbance wavelength	***Size (nm)***	***Disc AgNPs absorbance wavelength***	***Size(nm)***
535 nm	24.4 nm	515 nm	37.8 nm
540 nm	28.2 nm	524 nm	43.8 nm
548 nm	31.3 nm	544 nm	50.7 nm
578 nm	32.7 nm	555 nm	58.8 nm
596 nm	37.8 nm	564 nm	68.1 nm
688 nm	43.8 nm	637 nm	106 nm
761 nm	50.7 nm	651 nm	122 nm

Looking at the tables, it was observed that the particle sizes of the silver nanoparticles increases as the absorbance wavelength increase. The size measurement of the spherical silver nanoparticles at 394 nm could not be performed due to the measurement capacity of the device.

4.5. STEM Analysis

The size and image of the spherical silver nanoparticles were investigated by STEM. The approximate size was measured 5 nm. Figure 4.12 shows the STEM image of spherical silver nanoparticle.

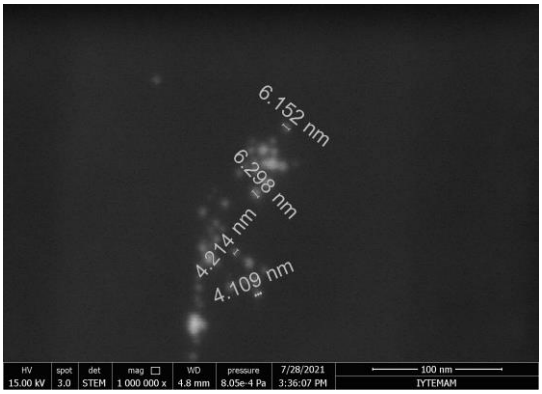

Figure 4.12. STEM image of spherical silver nanoparticle.

4.6. Nanoparticle Effect on LIBS Signal Intensity

Signal enhancement from the presence of spherical silver nanoparticles is known from literature studies and to make a comparison between spherical AgNP and different shapes and different absorbance AgNP was also studied in this thesis. When looking at the literature studies, generally 1-2 fold increase in signal was observed with spherical Ag nanoparticles (De Giacomo et al., 2013, 2014,2016).

In this study, the effect of the presence of spherical silver nanoparticles, with maximum absorbance at 394 nm, on the signal intensity of the Pb, is shown in Figure 4.13.

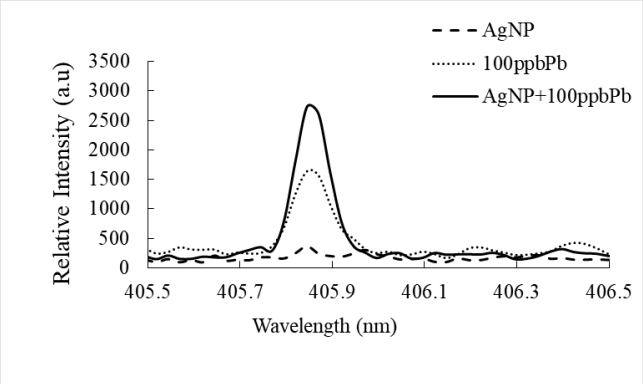

Figure 4.13. LIBS spectral regions representing the most prominent emission line of Pb(I) with and without spherical AgNP at t_d=2 μs t_g=900 μs laser energy=130 mj (4 single-shot accumulation)

Figure 4.14 shows the net LIBS signal enhancement Pb in the presence of spherical shape silver nanoparticles.

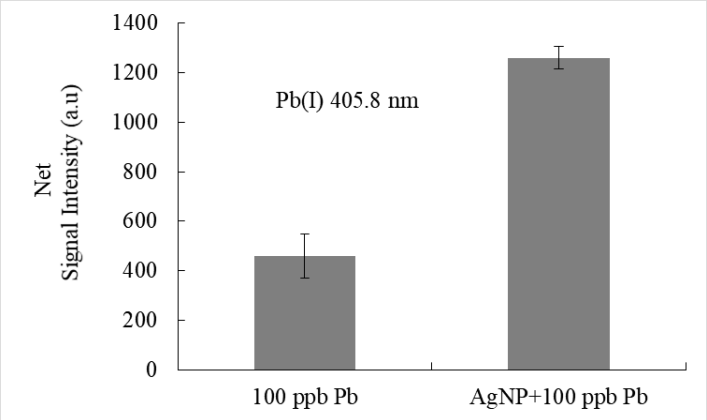

Figure 4.14. Net LIBS signal of Pb(I) at 405.8 nm with spherical AgNP (at 394nm absorbance) (t_d=2 mcs t_g=900 mcs laser energy=130 mj ,4 single shot accumulation).

Results indicate approximately 2.5-3 times an increase in signals, in the presence of spherical NPs.

Looking at the results, the signal enhancement provided by the spherical silver nanoparticles was very close to the signal enhancement observed in the literature (De Giacomo et al., 2013; 2014; 2016). As a result of this preliminary work, studies continued with silver nanoparticles with absorbances at different wavelengths. The spectra are given in Figure 4.15 and figure 4.16 show the effect of the disc and prism silver nanoparticles of different sizes, respectively, on the LIBS signal intensity of Pb(I) at 405.78 nm.

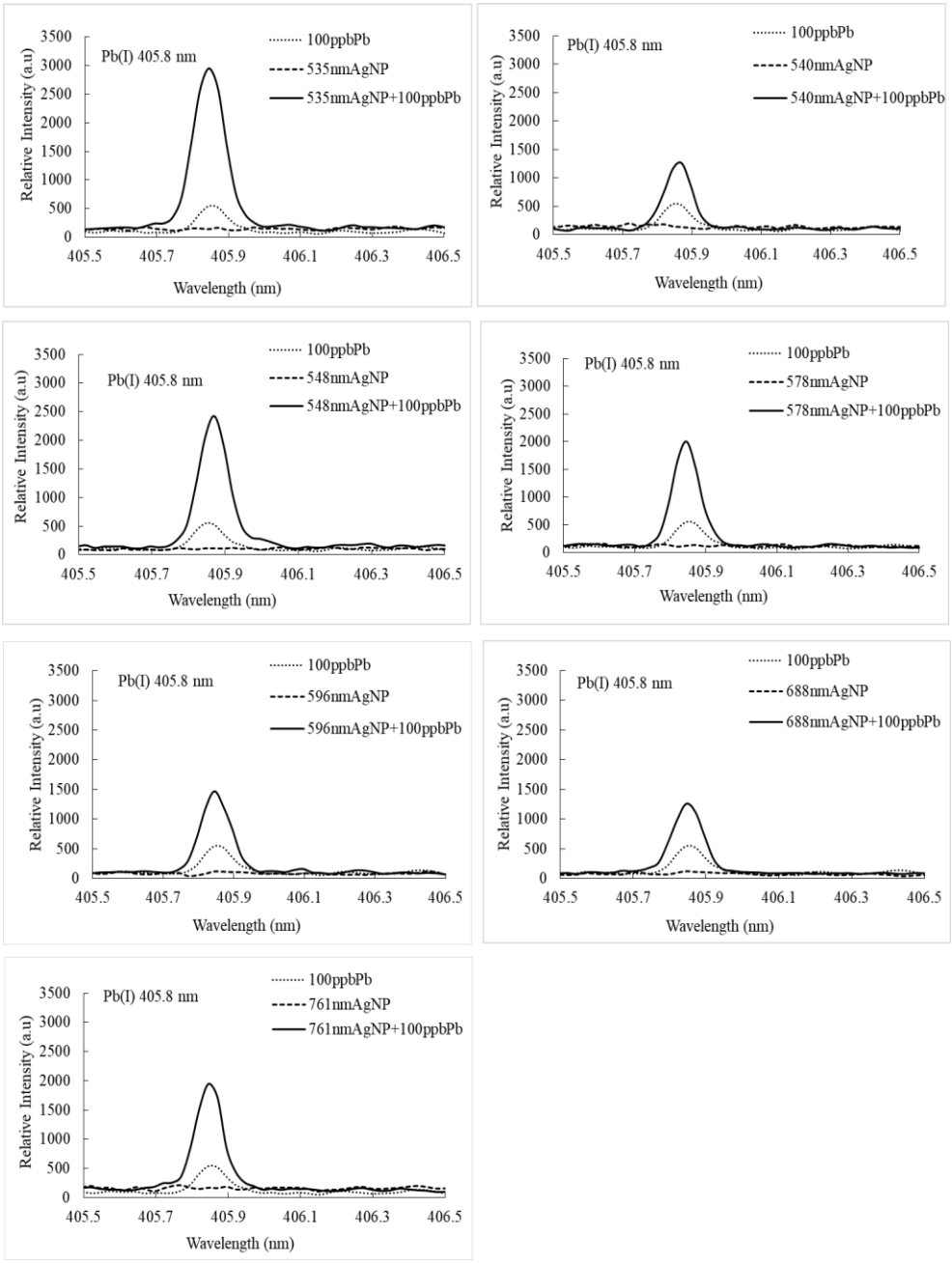

Figure 4.15. LIBS spectrum for Pb(I) heavy metal at 405.8 nm emission line with prism-shaped Ag nanoparticles with absorption wavelengths at td=2 us tg=900 us laser energy=130 mj (4 single-shot accumulation)

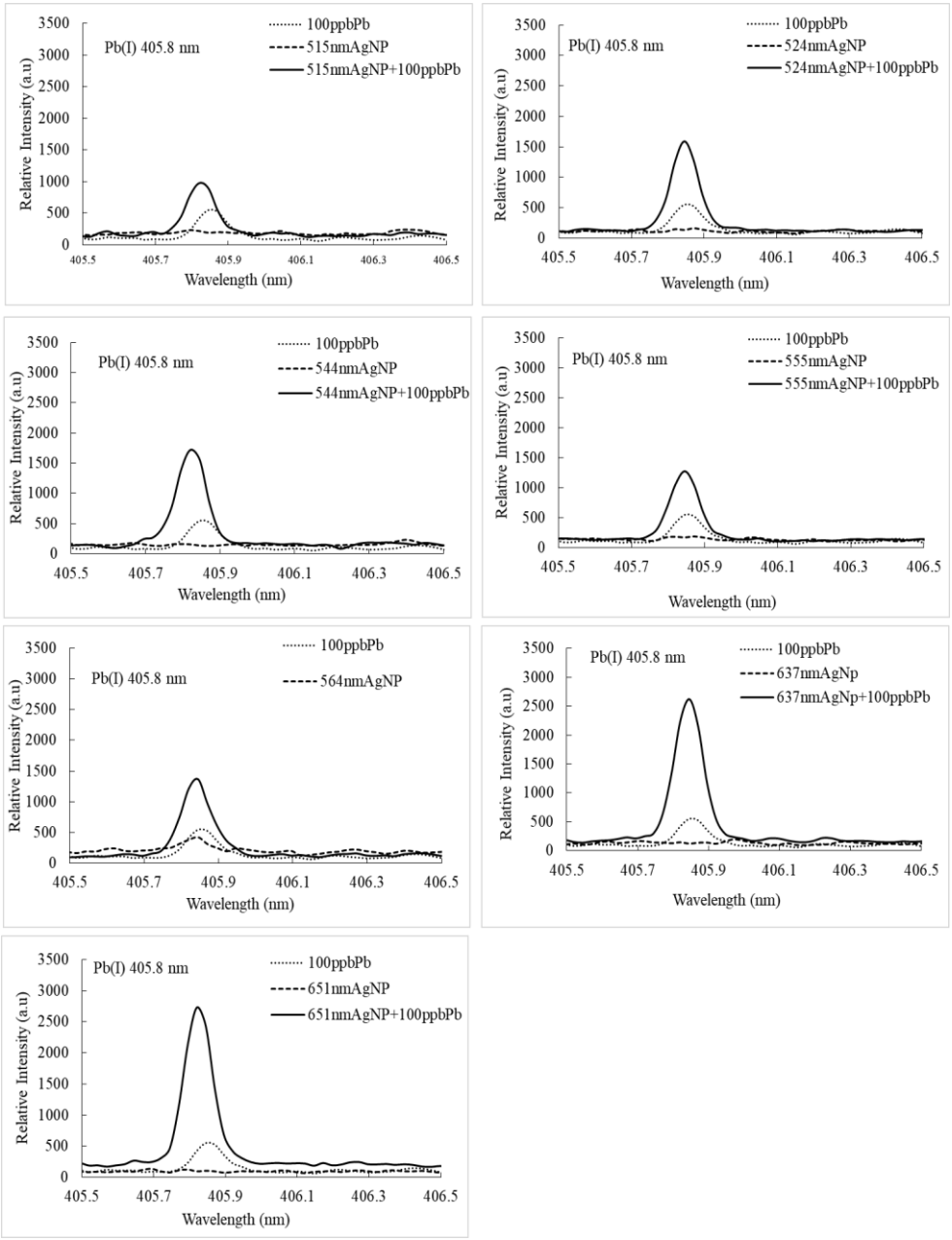

Figure 4.16. LIBS spectrum for Pb(I) heavy metal at 405.8 nm emission line with disc-shaped Ag nanoparticles at td=2 us tg=900 us laser energy=130 mj (4 single-shot accumulation)

Figure 4.17 shows the net signal enhancement for Pb in the prescence of silver nanoparticle, which has a (a) prism and (b) disc shape and different absorbances nm, with LIBS.

(a)

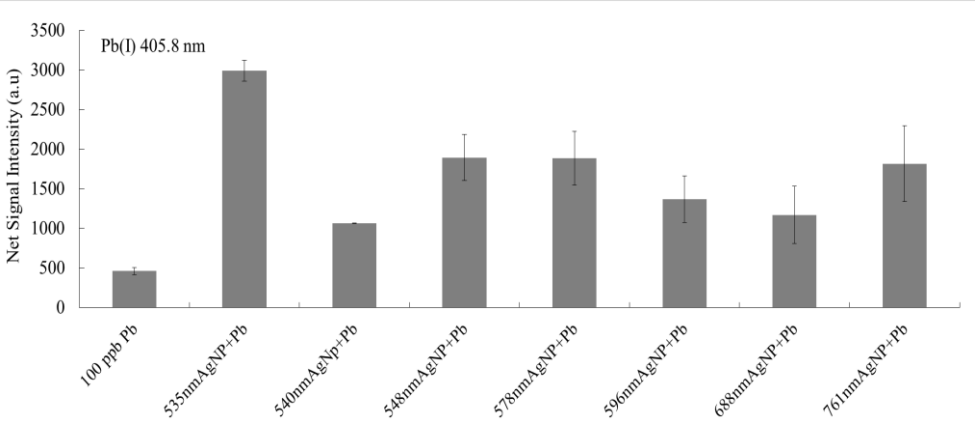

(b)

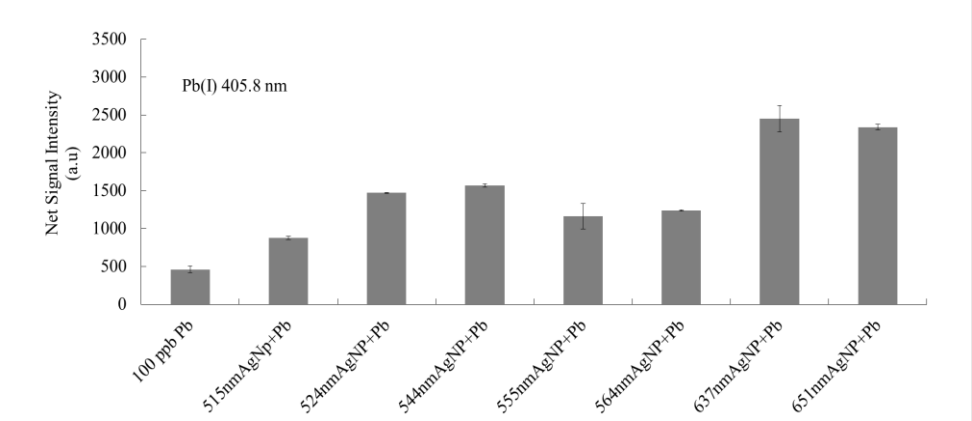

Figure 4.17. Net LIBS signal of Pb(I) at 405.8 nm with a) prsim and b) disc shape AgNP (at different nm absorbance) (t_d=2 μs t_g=900 μs laser energy=130 mj, 4 single shot accumulation).

Table 4.2 shows the enhancement factor on the LIBS signal intensity of the 100 ppb Pb (I) element of the prism and disc-shaped silver nanoparticles. The 100 ppb Pb (I) signal intensity without the nanoparticle is 500 a.u.

Table 4.2. Enhancement factor at Pb(I) 405.8 nm with nano prisms and nanodisc Ag nanoparticle.

Prism AgNP (Absorbance λ)	Enhancement Factor	Disc AgNP (Absorbance λ)	Enhancement Factor
535 nm	6	515 nm	1.6
540 nm	2	524 nm	3
548 nm	4	544 nm	3.4
578 nm	4	555 nm	2.6
596 nm	3	564 nm	2.8
688 nm	2.4	637 nm	4.6
761 nm	3.6	651 nm	4.4

As a result of the studies carried out, silver nanoparticles in prism shape with a wavelength of 535 nm showed the highest increase. Silver nanoparticles with 535 nm absorbance, which is the closest wavelength to the laser light source used in the experiment with a wavelength of 532 nm, achieved 6 times improvement in the signal intensity. These two nm sources, which are very close to each other, match each other very well and increase the free-electron induction, so the ablation threshold is lowered, and the observed signal increase. While the 532 nm laser source is itself a source to excite the atoms in the sample, it is thought that another power source comes at 535 nm. The system here is considered to be the same as laser-induced fluorescence LIBS (LIF-LIBS) (Loudyi et al., 2009). The working principle ın LIF-LIBS the advantage of combining two pulses. Due to the proximity of these two nm sources to each other, matching makes them behave like a single excitation source. Thanks to the proximity of the 532 nm laser light source to the 535 nm absorbance, the plasmons formed on the surface of the nanoparticles strongly interact with the electromagnetic field of the laser, resulting in the highest increase in the signal.

Also, scattering increases as particle size increases (Skoog et al.,2007). Looking at Table 4.1, it is seen that the smallest particle size is a prism-shaped nanoparticle with an absorbance of 535 nm. Thanks to this small size, absorption is

more assumed than other nanoparticles without scattering. Thanks to this good absorption mechanism, the laser light is absorbed very well by the nanoparticles. The heat created by this strong absorption causes rapid heating that will pass directly into the vapor phase without transition from solid to liquid. Due to the rapid heating of the substrate material, this phase transition mechanism can help easily transfer the analyte for more efficient evaporation, atomization, and excitation. And this is of great importance among the reasons for the increase in signal. But even if the loaded concentration of all nanoparticles is the same, how the dispersions are located on the surface while loading the wafer is a question mark. This can cause the distances between nanoparticles to vary disproportionately with size. This is another proof that the improvement in signal changes regardless of size. According to the recent studies in the literature, it was concluded that the surface concentration should not be kept constant while analyzing the LIBS signal intensity of nanoparticles in terms of size relationship (Salajkova et al., 2021).

Looking at the result, prism nanoparticles do not fully correlate with the size of the signal. Disc silver nanoparticles were synthesized by heating the prism silver nanoparticles, they became disc-shaped and they wanted to go to the most stable thermodynamically. This event made disc silver nanoparticles more stable than prism silver nanoparticles. When working with high laser pulses, prism silver nanoparticles cannot withstand these pulses and heat and can slide back towards spherical silver nanoparticles. Another explains that the increase in signal levels can vary without proportion to size. Thanks to the more stable structure of the disc silver nanoparticles and their resistance to laser pulses, their structure does not deteriorate and the signal improves as the size (i.e., absorbance wavelength) increases. For this, STEM analysis was performed with prism-shaped silver nanoparticles with maximum absorbance at 535 nm. Figure 4.18 shows the STEM image of prism-shaped nanoparticles.

a) b)

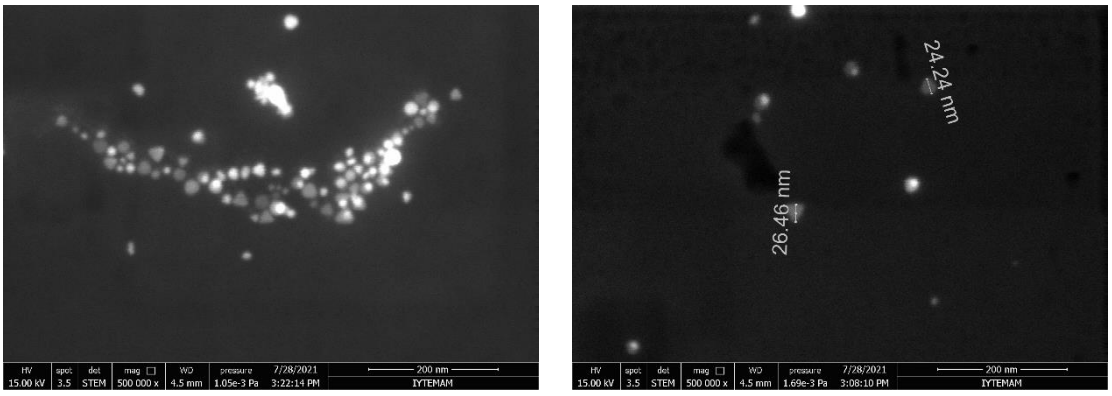

Figure 4.18. STEM image of prism shaped silver nanoparticles with maximum absorbance at 535 nm.

Looking at the STEM images, it is seen that the prism-shaped silver nanoparticle shifts to the spherical-shaped nanoparticle at some points. In addition, thanks to the STEM image, it has been proven once again that the average size of the prism-shaped silver nanoparticle is around 24 nm.

4.6.1. Calibration Graphs and Analytical Figures of Merits

To determine the applicability of NELIBS technique studies with AgNP nano prisms with 535 nm absorbance, studies were carried out on a calibration graph for quantitative analysis of Pb heavy metal elements.

Calibration standards for Pb element were prepared from its stock solutions by serial dilutions with distilled water. While working with calibration graphs, the detector delay time is set to 2 microseconds, the gate time to 900 microseconds, and the laser energy to 130 mJ. Calibration charts were constructed using the most sensitive neutral emission line of Pb (I) 405.78 shown in figure 4.19. At a concentration range from 1 μg L^{-1} to 100 μg L^{-1} Pb a linear correlation was with R^2=0.98 (only Pb) and R^2=0.99 (with AgNP with 535 nm absorbance). An increase in the correlation coefficient was observed in the presence of nanoparticles.

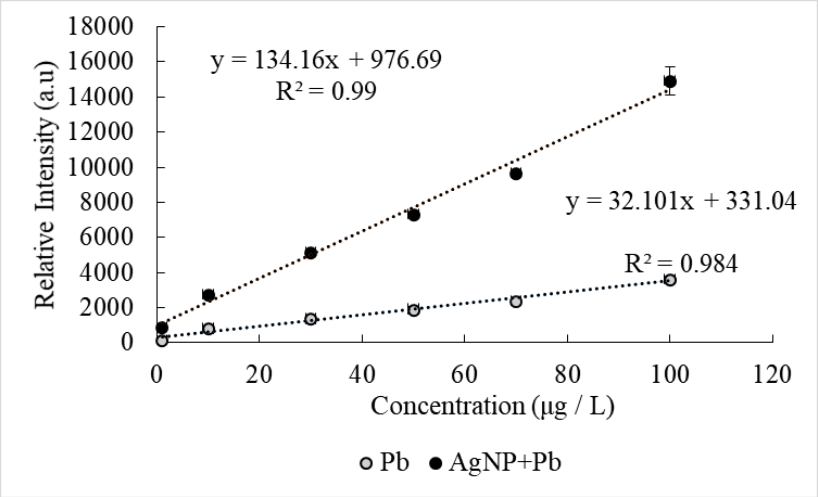

Figure 4.19. Calibration graph for Pb(I) using 405.78 nm emission line under optimum instrumental conditions.

At higher concentrations, there is an increase in error bars. These changes due to self-absorption at high concentrations are normal in LIBS studies.

When looking at the calibration study, it is seen that the linearity is higher when working with 535 nm silver nanoparticles than when working with the Pb element alone. It also proves that the studies performed with 535 nm Ag nanoparticles have higher sensitivity in terms of LIBS experiments.

Detection limit calculations were made using a calibration chart. The net peak height of the emission signal is used to calculate the detection limit. Calculation of the lowest concentration level that can be observed using the most reliable level known is called the detection limit (*DL*) (Ingle and Crouch, 1998). Its formula is 3 times the standard deviation (σ) of the backgrounds for the lowest analyzed concentration level on the calibration graph divided by the slope (m) of the calibration graph.

$$DL=3\sigma/m$$

The detection limit for Pb was calculated as 1,64 ppb, 0.82 picograms (pg) by using the detection limit formula and using the lowest concentration (1 µg / L) observed on the calibration graph. Looking at our group's previous LIBS study (Aras and Yalçın,2019), it was seen that there was an improvement in the presence

of silver nanoparticles with 535 nm absorbance at the detection limit calculated as 11 pg for the Pb heavy metal. When looking at other studies in the literature, a detection limit of 136 ppb levels was found for Pb (Yang et al., 2017). When we look at the recent literature studies, 0.5 ppm test and limit were calculated for lead metal (Haider et al., 2021).

In the presence of silver nanoparticles with an absorbance of 535 nm, not only the signal intensity but also the signal-to-noise ratio was examined. The signal is found by subtracting the backgrounds from the signal height. Noise is expressed as 3 times the standard deviation of the backgrounds. Table 4.3 shows the S / N ratios without nanoparticles and in the presence of nanoparticles

Table 4.3. S/N ratio of Pb line 405.8 nm in the presence of AgNPs with various absorption wavelengths

	S	N	S/N 405.8 nm Pb(I)		S		S/N 405.8 nm Pb(I)
100 ppb Pb	460.4	69.5	6.6	AgNP λmax:761 nm	1816.6	7.4	23.5
AgNP λmax:394 nm	1260.3	164.9	7.6	AgNP λmax:515 nm	877	9.3	14.8
AgNP λmax:535 nm	2993.5	55.4	54.0	AgNP λmax:524 nm	1469.3	4.0	23.0
AgNP λmax:540 nm	1065.5	33.1	32.2	AgNP λmax:544 nm	1568.1	09.7	14.3
AgNP λmax:548 nm	1893.3	59.4	31.9	AgNP λmax:555 nm	1160.0	2.0	36.2
AgNP λmax:578 nm	1887.6	80.8	23.4	AgNP λmax:564 nm	1237.8	8.0	14.1
AgNP λmax:596 nm	1368.5	97.2	14.0	AgNP λmax:637 nm	2448.2	0.2	40.6
688 nm abs. AgNP	1170.5	39.2	29.9	681 nm abs. AgNP	2336.5	25.0	18.7

When the ratio is more than 1: 1, the signal is more than noise. When looking at all S / N ratios, there is an improvement in S / N ratios in the presence of nanoparticles. The highest S / N ratio was calculated as 54.04 in the presence of silver nanoparticles with the 535 nm absorption wavelength. Figure 4.20 shows the emission spectra with and without AgNP.

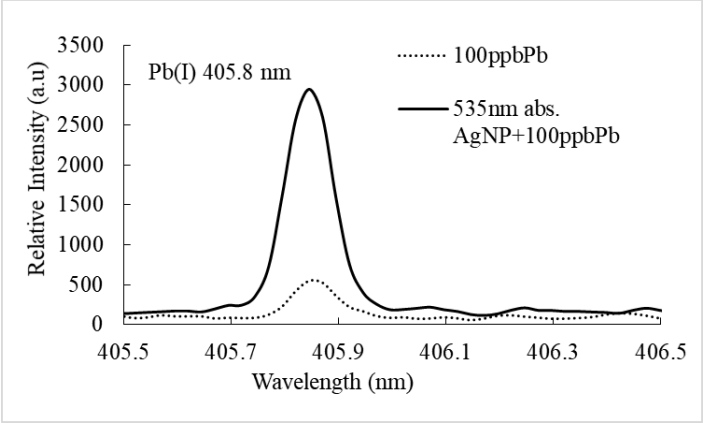

Figure 4.20. Pb emission spectra with and without prism-shaped AgNP with λ_{max} 535 nm under optimized experimental conditions

When looking at Figure 4.20, it is seen that in the presence of AgNP with 535 nm absorbance, there is not only an increase in the signals but also a decrease in the backgrounds.

4.6.2. The effect of Nanoparticle Concentration

In the experiments, the volume of droplets loaded on the silicon nitride layer is 500 nanoliter in volume. To investigate the effect of the concentration of applied nanoparticles, experiments were carried out by dropping prism AgNP with an absorbance of 535 nm onto a silicon nitride wafer in different numbers of drops.

First of all, the signal was received with 10 mg L^{-1} Pb alone and the signal intensity was around 2000. Then, first, a single drop on the prism-shaped AgNP silicon nitride layer with an absorbance of 535 nm, then two drops in a row, then 3 drops in a row, 4 drops in a row, and finally 5 drops in a row ıt was dropped on silicon nitrate wafer and left to dry at room temperature. After AgNP drops dried, 10 ppm Pb heavy metal solution was dropped on it, and analyzes were carried out

with the dried drop LIBS method. Figure 4.21 shows the effect of the number of silver nanoparticle droplets on LIBS signal intensity.

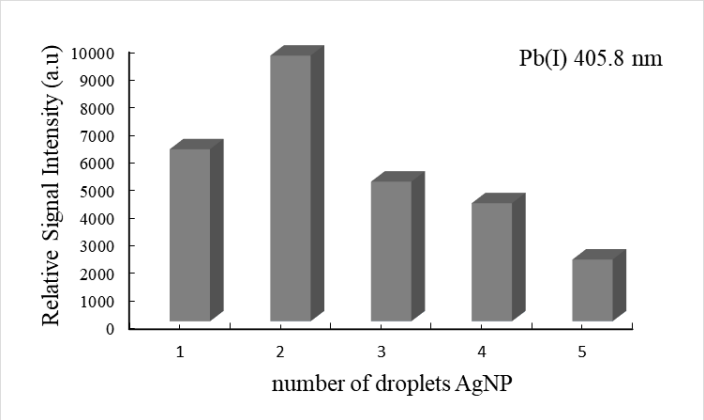

Figure 4.21. Effect of concentration of AgNP in the form of a prism with λ_{max} 535 nm on LIBS signal intensity with Pb element under optimized instrumental conditions.

Looking at the results, it was seen that more than 2 droplets of AgNP caused a decrease in the Pb (I) LIBS signal intensity. This may be due to self-absorption.

4.6.3. Order of Loading

The order of loading experiment has been carried out to observe whether the loading order affects. For this, first of all, 10 ppm Pb was dropped to the Si_3N_4 wafer layer and dried. After the Pb drop dries, the silver nanoparticle with an absorbance of 535 nm was dropped and left to dry at room temperature. Then, under appropriate experimental conditions, the analysis was carried out with a diffrent energy laser. To compare which loading order is better, experiments were carried out by dropping the first silver nanoparticle and then the Pb element. Figure 4.22 shows the experimental results of the order of loading the wafer substrate.

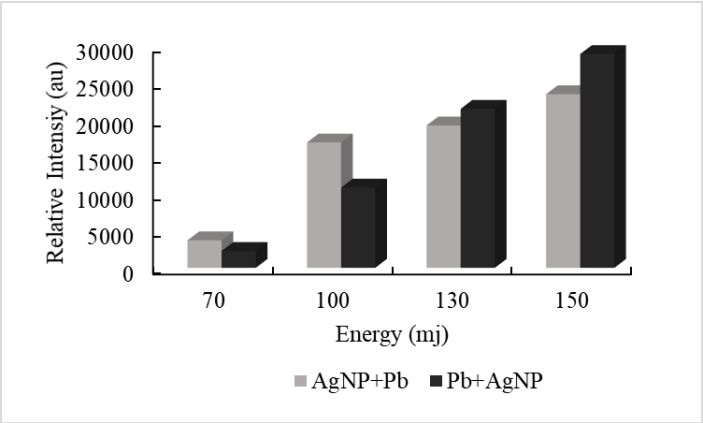

Figure 4.22. Load sequence experimental results under optimized instrumental conditions.

Looking at the results, there is a great link between the loading sequence and laser energy. It has been observed that the signal intensities are not good at low energy levels (low energy up to about 100 mj energy level) where the lead element is below the nanoparticle droplet (ie the Pb element is dropped first). Because at low energies, the underlying Lead element cannot be ablated. Energy is insufficient. At energy levels above 100 mj, even if the lead element is dropped first, the laser energy reaches the lead element and there are good levels of signal with the nanoparticles.

4.6.4. Preconcentration effect

The preconcentration effect was observed in the presence of silver nanoparticles with 535 nm absorbance. For this, silver nanoparticle was first dropped onto the silicon nitride layer and dried at room temperature. Then, a single drop of Pb solution, 2 drops of Pb solution, 3, 4, and 5 drops of Pb solution were dropped at separate points and dried. At this point, the signal increase is expected to vary in proportion to the number of Pb drops. For example, a 2-fold increase in signal increase is expected when two drops of Pb solution are dropped. The experiments were carried out with a 10 ppb amount of Pb solution. The reason why low concentration Pb is used here is that when the number of drops is increased, self-absorption that may come in high concentration is prevented. Figure 4.23 is the graph showing the preconcentration results of Pb.

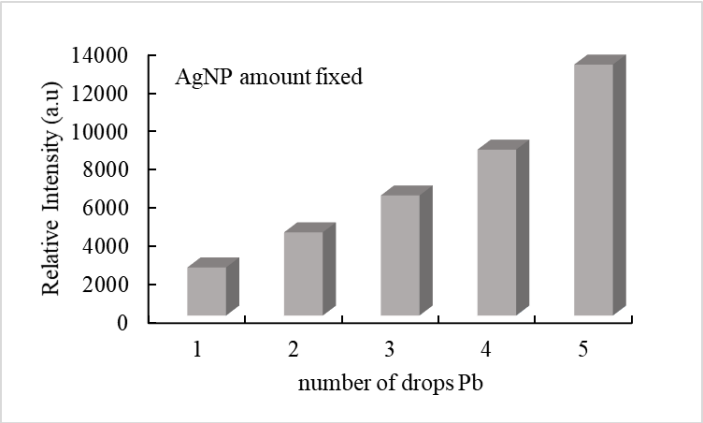

Figure 4.23. Effect of preconcentration on LIBS signal intensity in the presence of prism-shaped AgNP.

When looking at the results, the effect of preconcentration is seen in the increase of Pb until the last drops. The accuracy of the method has been proved thanks to this experiment performed in the presence of prism-shaped silver nanoparticles with an absorbance of 535 nm.

4.6.5. Applications on Reference Water Sample

To determine the accuracy and precision of the method, reference water samples were also studied. HPS standard solution was used for this. Figure 4.24 shows the experimental results with the HPS solution and the nanoparticle.

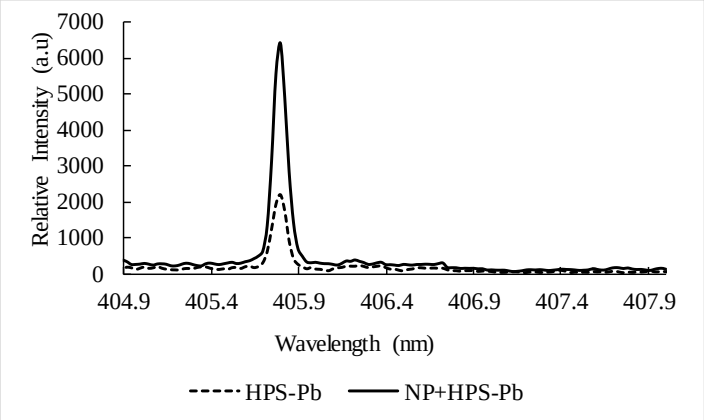

Figure 4.24. HPS standard solution with prism shaped silver nanoparticle experimental result.

When looking at the spectra in Figure 4.24, it was observed that 50 ppb Pb signals obtained by diluting the HPS standard solution were higher in the presence

of silver nanoparticles. A 2-2.5-fold increase in NELIBS signals was observed. The precision of the 535 nm absorbance NELIBS system is given in terms of %RSD for 50 µL concentration level and it is % 12.8. LIBS technique generally has low precision with %RSD value in a range of %5-%20. The result in this value range is an acceptable value in terms of precision.

The applicability of the 535 nm absorbance NELIBS method for quantitative analysis of Pb in environmental samples was evaluated using drinking water (OZSU) provided from a local market. Spiking experiments were used for method validation. In the drinking water of OZSU concentarations of the element of Pb level is below the detection limit of the 535 nm absorbance NELIBS method. For this purpose, the drinking water standard was spiked with four standard solutions of 15, 30, 50, 70 µg/L concentrations for Pb to achieve desired final concentrations. Then, analyte content was determined under optmized experimental conditions. The drinking water sample was also tested for Pb content by 535 nm absorbance NELIBS but no detectable signal was observed before spiking experiments. Figure 4.25 shows the experimental results of a) before spiking b) after spiking experiments results.

a) b)

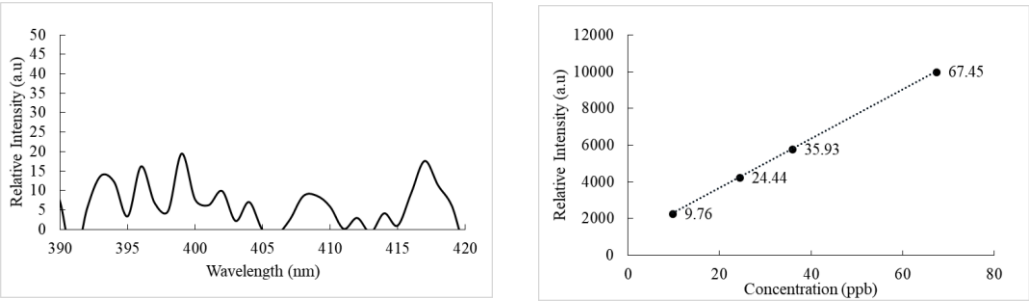

Figure 4.25 a) NELIBS spectrum of OZSU drinking water sample before spiking experiments b) NELIBS calibration graphs of drinking water sample after spiking experiments.

After the spiking experiments, recoveries were calculated for all concentrations with the help of equation in calibration graph of the figure 4.19. Percent recovery results from show in table 4.4.

Table 4.4 Recovery results from the drinking water samples spiked with a single element standard solutions with four different concentrations.

Drinking water, OZSU, µg/L	% Recovery ± SD
15	65 % ± 15.9
30	81.46 % ± 11.84
50	71.84 % ± 19.26
70	96.36 % ± 6.30

Looking at the percent recovery results for all concentrations of drinking water recovery results within 20% standard deviation were obtained. 70 µg/L was among the best, with recoveries higher than 95%. Although standards and samples are prepared at the same time, there may have been fluctuations in percent recovery according to concentrations, as the calibration standards were analyzed beforehand. The recovery results that are not too high are also due to the inhomogeneity of the plasma and the matrix effect in the drinking water. This subject is among the subjects that require more detailed study. According to the World Health Organization, the acceptable amount of lead element in drinking water is at the level of 10 ppb (Babaee et al., 2019). Thanks to spiking experiments, it is seen that it is possible to detect the lead element at this level with a silver nanoparticle with an absorbance of 535 nm.

4.7 NELIBS Studies with Chromium

After the experiments with the Pb, it was found that the silver nanoparticle with an absorbance of 535 nm had the highest effect on the signal intensity. As a result, experiments were carried out with silver nanoparticles with an absorbance of 535 nm together with the element of Chromium.

For NELIBS studies firstly, experiments were carried out for detector gate time, detector delay time, and laser energy, which are known as optimization parameters of the Cr element. Figure 4.26 contains the LIBS spectrum of the Cr element.

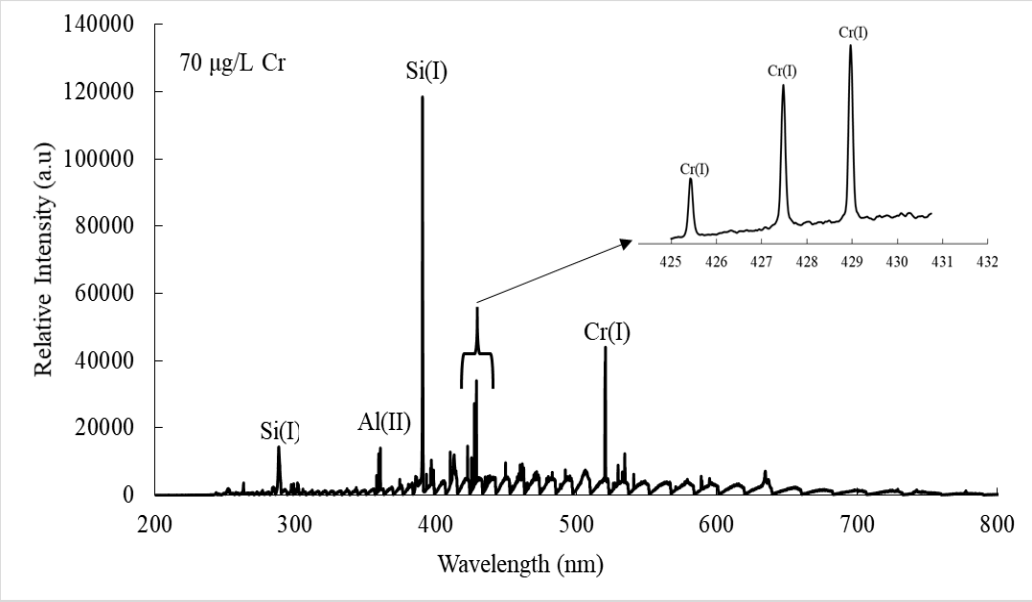

Figure 4.26. Typically LIBS spectrum of Cr(I) 425.4, 427.4, and 428.9 nm.

According to the spectrum in Figure 4.25, the Cr has a high signal intensity and optically thin at a wavelength of 428.9 nm. The transition at this wavelength is also seen as a Grotrian diagram in figure 4.27. Optimization studies were made based on this wavelength.

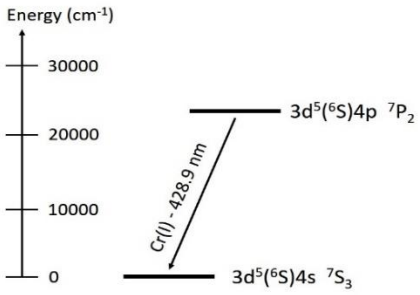

Figure 4.27. Grotrian Diagram for Chromium at 428.9 nm emission

Looking at the Grotrian diagram, it is seen that the Cr element emits from a single excited energy level to the ground level.

For the detector delay time, the experiments were carried out by keeping the detector gate with (22 μs) and laser energy (130 mj) parameters constant. Experiments were carried out by keeping the remaining parameters constant for detector gate time and laser energy optimizations. Figure 4.28 shows the results of the detector gate interval, detector delay time, and laser energy experiments.

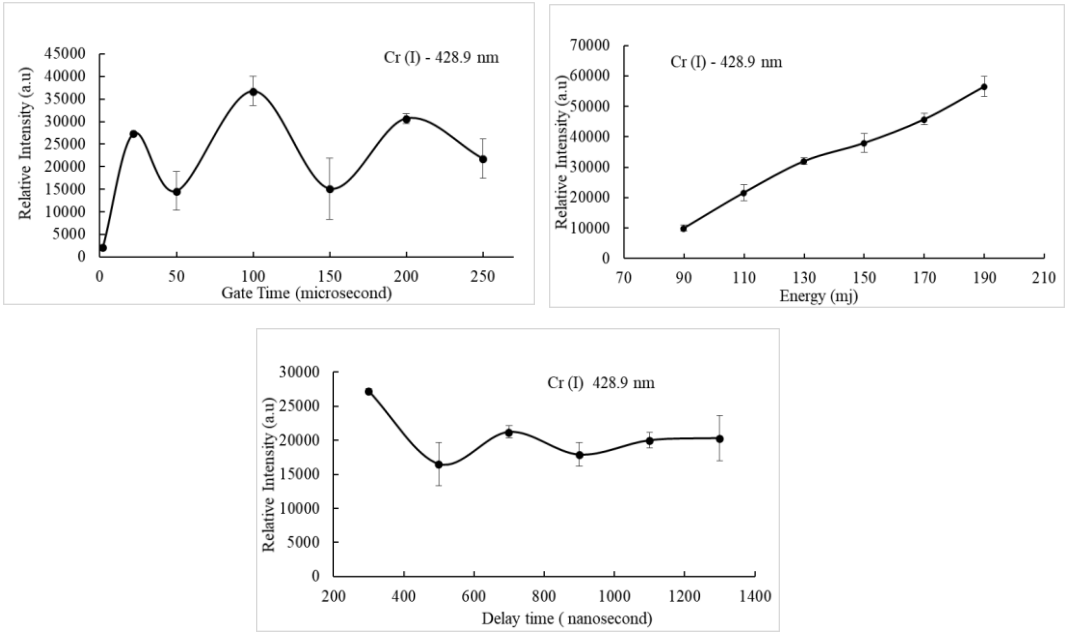

Figure 4.28. Optimization experimental studies of detector delay time, detector gate time, and laser energy for Cr(I) at 428.9 nm. Detector gain 100, 4 single shot accumulation, 70 ppb Cr.

As a result of optimization studies, for Cr heavy metal, the optimum delay time, the gate time, and the laser pulse energy was determined as 0.3 microseconds, 100 microseconds, and 130 mj, respectively. If both Cr and Pb are present in the sample, it has been observed that the emission peak can be observed in the other element, regardless of which element's parameter is entered. In a sample containing both Cr and Pb, analysis can be made by using the parameters of which element to be examined.

After the optimized detector parameters and laser energy value were found, nanoparticle studies were started with the Cr element. As with the Pb element, only one type of silicon nitride layer, which is Si_3N_4, is used. First, the 535 nm absorbance prism was dropped onto the silver nanoparticle wafer and left to dry at room temperature. After the silver nanoparticle drop dries, 70 ppb Cr heavy metal aqueous solution was dropped on it and left to dry at room temperature. After the drops dried, analyzes were carried out with 130 MJ laser energy. Figure 4.29 shows the results of these analyzes.

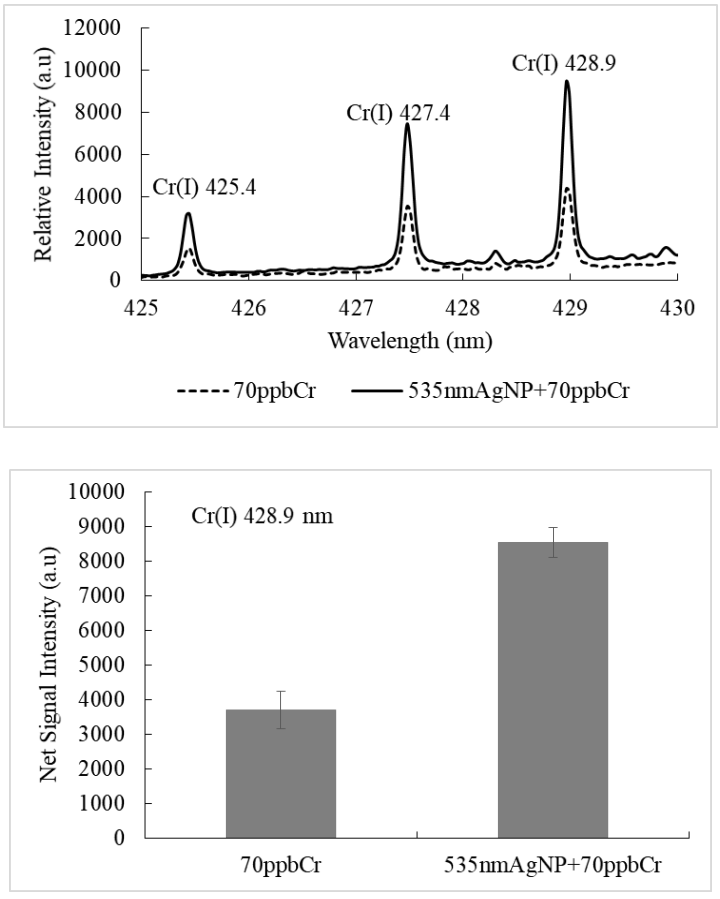

Figure 4.29. 12 Effect of 535 nm AgNPs on Cr LIBS signal intensity.

Considering the spectrum and net signals, a 3-3.5 fold increase in signal intensity was observed in the presence of nanoparticles. As with the Pb element, the silver nanoparticle with a maximum absorbance of 535 nm increased the LIBS signal intensity as an additional power source to the laser source. Again at this point, the working principle is accepted as LIFLIBS. When the laser light hits the wafer, it is thought that there is an increase in the signal due to the plasmons formed on the surface. While the particle number is less when there is only one Cr drop, the particle density increases with the nanoparticles. This increases the electron density and increases the signal.

Plasma temperature is an important parameter that gives valuable information about the elemental composition and emissivity of the plasma. There is a strong relationship between plasma temperature and emission intensity. Plasma temperature calculation was made for the change in plasma temperature in the presence of nanoparticles. Figure 4.30 (a), (b) shows plasma temperature graphs with and without nanoparticles.

a) b)

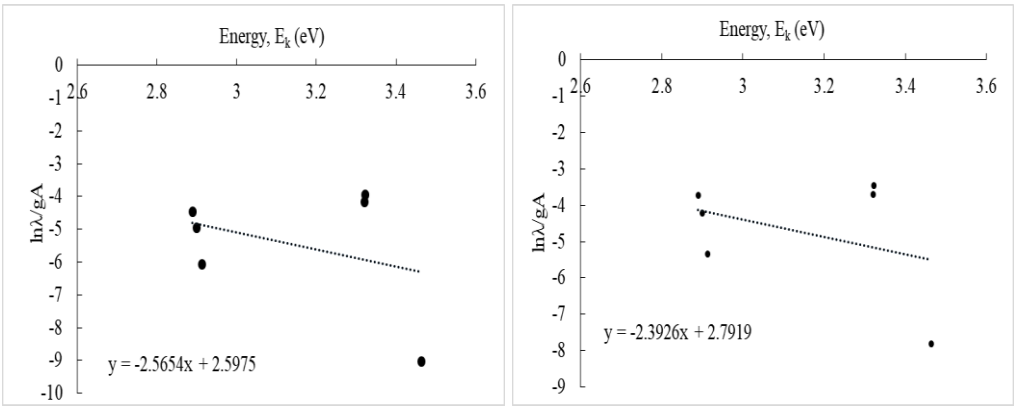

Figure 4.30. Typical Boltzmann plot that used for temperature calculation obtained from Cr lines a) without nanoparticle b) with 535 nm maximum absorbanca AgNPs.

From the slopes of these graphs, the plasma temperature without AgNP and with AgNPs was found to be 4523 K and 4850 K, respectively. When these two graphs are considered (Figure 4.30) it is seen that, it was observed that the plasma

temperature was higher in the presence of nanoparticles. It was found that the ionization was greater than the presence of nanoparticles. This is another reason for obtaining higher signal intensity in the presence of nanoparticles. It can be considered normal for the plasma temperature to be low due to the optimization conditions. In addition, the substrate being silicon nitride causes it to absorb the incoming laser beam very well and cool the plasma. In addition, nanoparticles absorb and use laser light very well, cooling the plasma. However, both the silicon nitride substrate and the nanoparticles provide an increase in the signal intensity by efficiently transferring the energy transfer to the sample.

McWhirter criterion was used to control the local thermal equilibrium (LTE) value. The energy difference between upper and lower levels for chromium line at 428.9 nm is 2.89 eV. Electron density is 2.59×10^{15} without AgNPs and 5.92×10^{17} with at 535 nm maximum absorbance AgNPs. Looking at the results, it was observed that the electron density was higher in the presence of nanoparticles. In addition, it was concluded that LTE conditions were met in the presence of nanoparticles. The increased electron density was another factor proving that the signal intensity was higher in the presence of nanoparticles.

To determine the detection limit, calibration charts were created with Cr element and Cr element in the presence of nanoparticles respectively. Figure 4.31 shows the calibration graph.

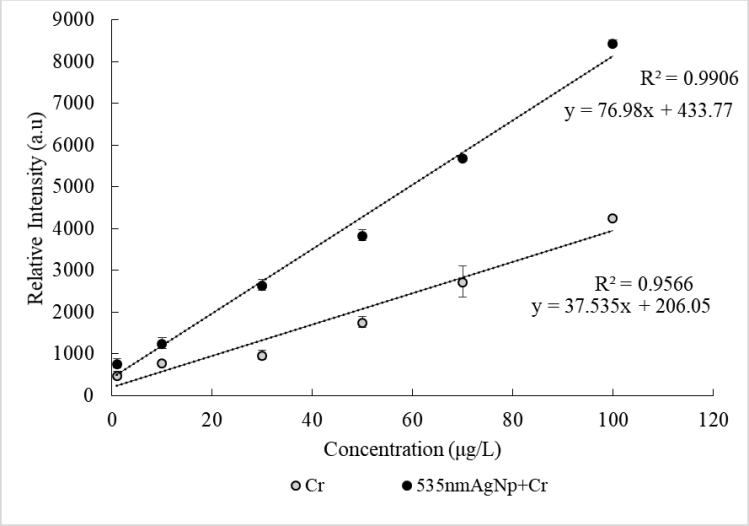

Figure 4.31. Calibration graph for Cr(I) 428.9 nm emission lines under optimized instrumental conditions.

When looking at the calibration graph, both the correlation coefficient and an increase in the slope are observed in the presence of nanoparticles. Detection limit calculations were made using the calibration graph of figure 4.31. Its formula is 3 times the standard deviation (σ) of the backgrounds for the lowest analyzed concentration level on the calibration graph divided by the slope (m) of the calibration graph. In the presence of a prism-shaped silver nanoparticle with an absorbance of 535 nm, the detection limit was calculated as 0.70 ppb (0.35 pg). When the literature studies are reviewed, it is seen that the detection limit of Cr heavy metal is reached at 18 ppb levels (Lee et al., 2012). In a study conducted in 2017, a detection limit of 16 ppb was found for the Cr element (Yang et al., 2017). Looking at the studies conducted in recent years, the detection limit for Cr heavy element was found at 25 ppb levels (Maji et al., 2021). Considering these results, an improvement is observed in ppb levels in the detection and limit for Cr heavy metal in the study conducted with Ag nanoparticles with 535 nm absorbance. In addition, the 1.5 pg detection limit calculated in the last study of our group became even better in this study with silver nanoparticles with 535 nm absorbance (Aras and Yalcin, 2019).

Analyzes were carried out with the reference water sample to determine the accuracy and workability of the method. HPS is used for this. Experiments were carried out according to the Cr concentration diluted to HPS reference water solution 70 ppb. Figure 4.32 shows the result of the experiment with HPS.

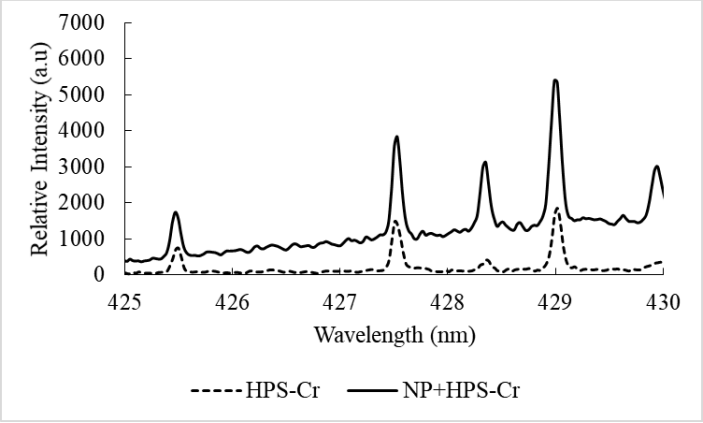

Figure 4.32 HPS DWPS solution with 535 nm absorbance silver nanoparticle experimental result

Looking at Figure 4.32, it is seen that there are a 3.2-fold increase in 70 ppb Cr LIBS signals despite the matrix effect in the presence of nanoparticles. Apart from that, emission wavelengths at 425.4 and 427.4 nm of element Cr reach the discrimination level as a strong peak in the presence of silver nanoparticles with 535 nm absorbance. In studies conducted by looking at reference water samples, it is seen that analysis can be done up to 70 ppb levels very easily. It is aimed to analyze the lower levels by repeating and improving the optimization studies.

The precision of the 535 nm absorbance NELIBS system is given in terms of %RSD for 70 μL concentration level and it is % 6.22. LIBS technique generally has low precision with %RSD value in the range of %5-%20. The result in this value range is an acceptable value in terms of precision.

The applicability of the 535 nm absorbance NELIBS method for quantitative analysis of Cr in environmental samples was evaluated using Riverine water (SLRS). Spiking experiments were used for method validation. In the riverine water concentration of the element of Cr level is near the detection limit of the 535 nm absorbance NELIBS method. For this purpose, the riverine water standard was spiked with four standard solutions of 10, 30, 50, 70 μg/L concentrations for Cr to achieve desired final concentrations. Then, analyte content was determined under optimized experimental conditions. The riverine water sample was also tested for Cr content by 535 nm absorbance NELIBS detectable signal was observed also before spiking experiments. Figure 4.33 shows the experimental results of a) before spiking and NP effect b) after spiking experiments results.

a) b)

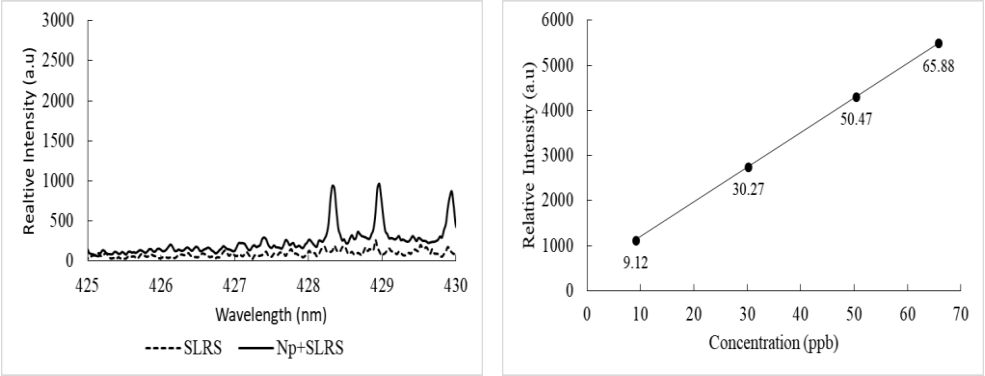

Figure 4.33 a) NELIBS spectrum of SLRS Riverine water presence of AgNP before spiking experiments and b) NELIBS calibration graphs of SLRS Riverine water after spiking experiments.

After the spiking experiments, recoviries were calculated for all concentrations with the help of equation in calibration graph of the figure 4.31. Percent recovery results in show in table 4.5.

Table 4.5 Recovery results from the riverine water samples spiked with a single element standard solutions with four different concentrations.

Riverine water, SLRS, µg/L	% Recovery ± SD
10	91.2 % ± 15.3
30	100.8 % ± 17.4
50	100.9 % ± 33
70	94.1 % ± 32.7

Looking at the percent recovery results for all concentrations of riverine water recovery results within 30% standard deviation were obtained. 70 uL-1 was among the best, with recoveries higher than 94. Considering the recoveries for the 30 and 50 ppb concentrations, it is seen that there is a high recovery. The reason for these high recoveries is due to high concentrations due to personal errors while preparing the solutions. Generally, it is known that there is Cr in groundwater below 1 ppb level (WHO 2019). When looking at the work done with Ag nanoparticles with an

absorbance of 535 nm, this level can be determined by looking at the detection limit results. Thanks to NELIBS spiking experiments, it is seen that it is possible to detect the chromium element at this level with a silver nanoparticle with an absorbance of 535 nm AgNP.

Although metal nanoparticles have contributed to the studies thanks to their unique properties such as large surface areas and interactions with metals, some problems have emerged in these studies. In this method, which works with the dry droplet method, it takes time to wait for the nanoparticle to be loaded and dried on a silicon nitride wafer first, then to wait for the drying process by dropping it in a heavy metal solution. In addition, drying the nanoparticles in a dark environment because of the possibility of deterioration due to exposure to light, further challenges the conditions of the experimental setup. The possibility of deterioration of nanoparticles due to exposure to light decreases the reliability of the analysis performed in the light environment during the experiment. It causes the efficiency of nanoparticles exposed to laser light to decrease in shot-to-shot experiments. The more unstable thermally structure of the prism nanoparticles may be another reason why the signals decline in experiments over time. One of the other reasons for obtaining relative signals in all experiments is that when loading the silicon nitride layer, there may be individual errors such as the correct point each time or the failure to get the same amount of solution each time.

CHAPTER 5

CONCLUSION

In this thesis, the effect of the presence of silver nanoparticles with different absorption wavelengths on LIBS signal intensity in the Pb element was investigated. Analyzes were carried out with the element Cr in the presence of silver nanoparticles whose absorbance wavelength was the most effective. The LIBS test set has not been changed due to the nanoparticle operation. LIBS instrumental parameters for example detector delay time, detector gate time, and laser energy are set according to the lead and chromium heavy metals. Then, experiments were carried out with silver nanoparticles using the dry droplet method. Calibration charts were created under appropriate experimental conditions at the peak emission wavelength of 405.78 nm for element Pb and 428.9 nm for Cr element. Under optimized experimental conditions, a LOD value of 1,16 and 0.69 ppb were obtained for Pb and Cr, respectively.

Silver nanoparticles have advantages such as high extinction coefficient, sharp extinction bands, high area enhancements. When silver nanoparticles interact with a certain wavelength of light, they release harmonic oscillations with the combination of the electromagnetic field of that light and the free electrons in the environment, and surface plasmon resonance occurs. The interaction of laser light with these surface plasmons provides a good optically improvement in metal surfaces. When the literature is reviewed, improvements in signal strength have been observed in analyzes with spherical nanoparticles. In this study, it was observed that nanoparticles with shapes different provide different rates of improvement on the signal intensity. It is known that nanoparticles with different shapes have absorbance at different wavelengths.

Looking at the results, the highest increase was observed when working with prism-shaped AgNP with 535 nm absorbance. Since the laser wavelength is close to the silver nanoparticle with an absorbance of 535 nm, it is thought that the plasmons formed on the surface of the nanoparticles are more powerful. Thanks to the interaction of these surface plasmons and the electromagnetic field of the laser

with each other, an increase in LIBS signals has been achieved. As in LIFLIBS studies, the silver nanoparticle with an absorbance of 535 nm acts as a second power source besides the 532 nm laser light.

The reason why the nanoparticle with maximum absorbance at 535 nm provides an increase in LIBS signal intensity is not only related to absorbance. In addition, this prism-shaped nanoparticle has a small size compared to other nanoparticles. Thanks to this small size, the absorption mechanism is more effective than the scattering mechanism. Thanks to the good absorption mechanism, the atomization process takes place in the most powerful way. In this way, the emission is ensured in the highest way.

In addition to these increases, thanks to the diagonal structures of the prism shape, the transmission of light between particles are much more effective. The effective realization of light ensures that the plasma is bright. This brightness of the plasma provides recovery in the form of effective signal enhancement in LIBS.

Plasma temperature with and without nanoparticles was calculated by using Cr element lines with the help of the Boltzman plot. It was found that the plasma temperature was higher in the presence of silver nanoparticles with maximum absorbance at 535 nm. High plasma temperature proves that the ionized part is more. Another explanatory reason why the signal intensity is higher than the presence of nanoparticles is that the plasma temperature is higher. In the electron density calculation made by using McWhirter conditions, it was found that the electron density was higher in the presence of nanoparticles. It was concluded that the increase in the signal intensity due to the presence of nanoparticles was due to the high electron density. In addition, it is observed that LTE conditions are provided more in the presence of nanoparticles, which proves the contribution of each species in the substance to the plasma.

In this thesis study, it was once again studied that the NELIBS technique can be performed in the heavy metal analysis without changing the experimental setup, and it has shown that the increase in the signal can be seen at different rates in nanoparticles with different shapes and wavelengths. It has been a guide for testing different types of nanoparticles with different shapes in LIBS studies in the future. Thanks to this study, it has been revealed that the relationship between nanoparticle

size and the nanoparticle concentration loaded on the wafer should be investigated. In addition, it is an important point in terms of nanoparticle production studies in investigating the reasons such as the nanoparticles being affected by light and deteriorating rapidly in room conditions.

REFERENCES

Abdelhamid, M.,. Attia Y. A., Abdel-Harith M., 2020. The significance of nano-shapes in nanoparticle-enhanced laser-induced breakdown spectroscopy. Journal of Analytical Atomic Spectrometry. 35: 2982-2989.

Aguirre M., Legnaioli S., Almod'ovar F., Hidalgo M., Palleschi V., Canals A.2013. Elemental analysis by surface-enhanced Laser-Induced Breakdown Spectroscopy combined with liquid–liquid microextraction . *Spectrochim. Acta B*: 79 ,88–93.

Alamelu D., Sarkar A., Aggarwal S., 2008. Laser-İnduced Breakdown Spectroscopy For Simultaneous Determination Of Sm, Eu And Gd İn Aqueous Solution. *Talanta.*77 :256– 261.

Anabitarte F., Cobo A., and Lopez-Higuera J. M. 2012. Laser-Induced Breakdown Spectroscopy. *Fundamentals, Applications, and Challenges* . 12

Aras N. , Ünal S., Arıca D. , Yalçın Ş., 2012. Ultrasonic nebulization-sample introduction system for quantitative analysis of liquid samples by laser-İnduced breakdown spectroscopy. *Spectrochimica Acta Part B*: Atomic Spectroscopy. 74-75, 87-94.

Aras, Yalçın. 2019. Investigating silicon wafer based substrates for dried-droplet analysis by Laser-Induced Breakdown Spectroscopy. *Spectrochimica Acta Part B*:152: 84–92

Babaee S., Hosseini S. G., Mirzaei M., 2019. Rapid and selective extraction of trace amount of Pb(II) in aqueous samples using a magnetic ion-imprinted polymer and detection by flame atomic absorption spectrometry, *Eclética Química,* 44: 73-84.

Bae D., Nam S., Han S., Yoo J., Lee Y., 2015. Spreading A Water Droplet On The Laser- Patterned Silicon Wafer Substrate For Surface-Enhanced Laser-Induced Breakdown Spectroscopy, *Spectrochimica Acta Part B*: Atomic Spectroscopy. 113, 70–78.

Balci F., Sarisozen S., Polat N., and Balci S., 2019. Colloidal Nanodisk Shaped Plexcitonic Nanoparticles with Large Rabi Splitting Energies. J. *Phys. Chem.* 123:26571-26576.

Bekefi, G. 1976. *Principles of Laser Plasmas.* New York: John Wiley & Sons. Inc.

Cahoon E. M., Almirall J.R., 2012. 'Quantitative Analysis of Liquids from Aerosol and Microdrops Using Laser Induced Breakdown Spectroscopy. *Anal.Chem*.84(5) : 2239-2244.

Chen Z., Li H., Liu M., Li R. 2008. Fast And Sensitive Trace Metal Analysis İn Aqueous Solutions By Laser-İnduced Breakdown Spectroscopy Using Wood Slice Substrates. *Spectrochim. Acta B:* 63: 64–68.

Chen G., Yang G.,, Ling Z., *a, Yang Y., Zhan Y., Jin X., 2021. The parameter optimization of lasers' energy ratio of the double-pulse laser induced breakdown spectrometry for heavy metal elements in the soil. The Royal Society of Chemistry Anal. Methods, 13: 1502–1510.

Contra Costa College Lawrence Hall of Science collaboration Spring. 2013 Interdisciplinary Study of silver nanoparticles filtration. Why nano-materials have different properties than bulk materials. *Engin.* 230. Introduction to Circuit Analysis.

Costa V., Aquino F., MarcioParanhos C., Filhoa E. 2017. Identification And Classification Of Polymer E-Waste Using Laser-İnduced Breakdown Spectroscopy (LIBS) And Chemometric Tools. *Polymer Testing*. 59: 390-395.

Cremers, D. A., and Radziemski. 2006. Handbook of Laser-Induced Breakdown Spectroscopy. *England* :John Wiley& Sons. Inc.

Dalyander P.S., Gornushkin I.B.,.Hahna W. 2008. Numerical Simulation Of Laser-İnduced Breakdown Spectroscopy: Modeling Of Aerosol Analysis With Finite Diffusion And Vaporization Effects. Spectrochimica Acta Part B: Atomic Spectroscopy, 63(2): 293-304.

Davıd W. Hahn And Nıcolo Omenetto. 2010. Laser-Induced Breakdown Spectroscopy (LIBS), Part I: Review of Basic Diagnostics and Plasma–Particle Interactions:Still-Challenging Issues Within the Analytical Plasma Community. *Applıed Spectroscopy* , 64(12): 335-66.

Dávid J., Palástia D., Albrychtc P., Janovszkya P., Paszkowskac K., Geretovszkyb

Z.,Galbácsa G. 2020. Nanoparticle Enhanced Laser İnduced Breakdown Spectroscopy Of Liquid Samples By Using Modified Surface-Enhanced Raman Scattering Substrates . *Spectrochimica Acta Part B*: 166 105793.

De Giacomo A., Gaudiuso R., Koral C., Dell'Aglio M., De Pascale O. 2013. Nanoparticle-Enhanced Laser-Induced Breakdown Spectroscopy of Metallic Samples. *Anal. Chem.* 85: 10180−10187.

De Giacomo A., Dell'Aglio M., Gaudiuso R., Korala C. and Valenza G. 2016. Perspective On The Use Of Nanoparticles To İmprove LIBS Analytical Performance: Nanoparticle Enhanced Laser İnduced Breakdown Spectroscopy (NELIBS). *JAAS*. 31:1566-1573.

De Giacomo A. Koral C., Valenze G., Gaudiıuso R., .. Dell'Aglio M. 2016.Nanoparticle Enhanced Laser-Induced Breakdown Spectroscopy for Microdrop Analysis at subppm Level. Anal. Chem. 88: 5251−5257.

De Giacomo A.. Dell'Aglio M., Alrifai R. 2018. Nanoparticle enhanced laser induced breakdown spectroscopy (NELIBS). *Spectrochim. Acta B:* 148: 05– 112.

De Giacomo A.. Dell'Aglio M., Alrifai R. 2018. Nanoparticle Enhanced Laser İnduced Breakdown Spectroscopy (NELIBS). *Anal. Chem.* 85 (21): 10180–10187.

Dell'Aglio M.,Salajková Z., Mallardi A.,Mezzenga Hag L., Cioffi N., Palazzo G., De Giacomo A. 2019. Application of gold nanoparticles embedded in the amyloids fibrils as enhancers in the laser induced breakdown spectroscopy for the metal quantification in microdroplets. Spectrochimica Acta Part B: Atomic Spectroscopy 155: 115-122.

Gaudiuso R., Dell'Aglio M., De Pascale O., Senesi G. and De Giacomo A. 2010. Laser Induced Breakdown Spectroscopy for Elemental Analysis in Environmental,Cultural Heritage and Space Applications: *A Review of Methods and Results, Sensors* .10(8): 7434-7468.

Gallou G., Sirven J. B., Dutouquet C., Le Bihan O., Frejafon E. 2011. Aerosols Analysis by LIBS for Monitoring of Air Pollution by Industrial Sources. Aerosol Science and Technology. 45: 918-926.

Godwal Y., Taschuk M.T., Lui S. L., Tsui Y.Y. and Fedosejevs R. 2008. Development Of Laser-İnduced Breakdown Spectroscopy For

Microanalysis Applications. *Laser and Practical Beams.* 26(1): 95-104.

Guangmen G., Jie W., Fang B., Di T., Quingwen F., 2016. A Hydrogel's Formation Device for Quick Analysis of Liquid Samples Using Laser-Induced Breakdown Spectroscopy' Plasma Science and Technology. 18(6): 661-665.

Haider, A.F.M.Y., Parvin, M., Khan, Z.H. et al., 2021. Highly Sensitive Detection of Lead in Aqueous Solution using Laser-Induced Breakdown Spectroscopy Coupled with Adsorption Technique. *J Appl Spectrosc.* 01125-3.

Huang J. , Ke C., Lin C. 2004. Matrix Effect On Emission/Current Correlated Analysis In Laser-İnduced Breakdown Spectroscopy Of Liquid Droplets. *Spectrochimica acta Part B:* 59(3) : 321-326.

Huang T., and Xu X., 2010. Synthesis And Characterization Of Tunable Rainbow Colored Colloidal Silver Nanoparticles Using Single-Nanoparticle Plasmonic Microscopy And Spectroscopy. *Journal of Materials Chemistry*. 20: 9867–9876.

Ingle JD, Crouch SR, Lafferty KM. 1998. *SpectrochemicalAnalysis.* New Jersey, USA: Prentice Hall.

Jolivet L., Leprince, M., Moncayo S., Sorbie L., Lienemann C. P., Motto-Ros V. 2019. Review Of The Recent Advances And Applications Of LIBS-Based Imaging *Spectrochimica Acta Part B:* Atomic Spectroscopy. 151: 41-53.

Khodashenas B., RezaGhorbani H. 2019. Synthesis Of Silver Nanoparticles With Different Shapes. *Arabian Journal of Chemistry*. 12(8): 1823-1838.

Kiris V.V., Butsen A.V.Ershov-PavlovE.A.,Nedelko M.L. and NevarA.A., 2019. Nanoparticle-Enhanced Laser Induced Breakdown Spectroscopy Using Copper Silver and Nickel–Carbon Nanocomposites on Aluminium. *International Journal of Nanoscience* .18.

Kumar A., Yueh F.Y., Miller T., Singh J.P., 2003. Detection Of Trace Elements In Liquids By Laser-İnduced Breakdown Spectroscopy With A Meinhard Nebulizer. *Applied Optics.* 42(30): 6040-6046.

Kumar A.,Yueh F.Y., Singh J.P. 2003. Double-Pulse Laser-İnduced Breakdown Spectroscopy With Liquid Jets Of Different Thicknesses. *Applied Optics*. 42(30):6047-6051.

Lee Y., Oh S.W., Han S.H., 2012. Laser-İnduced Breakdown Spectroscopy (LIBS) Of Heavy Metal İons At The Sub-Parts Per Million Level İn Water. *Appl. Spectrosc*.66(12): 1385–1396.

Liu J., He H. , Xiao D., Yin S., Ji W., Jiang S., Luo S., Wang B., and Liu Y., 2018. Recent Advances of Plasmonic Nanoparticles andtheir Applications. *Materials* 11: 1833.

Loudyi H., Rifa K., Laville S., Vidal F., Chakera M., Sabsabi M., 2009. Improving laser-induced breakdown spectroscopy (LIBS) performance for iron and lead determination in aqueous solutions with laser-induced fluorescence (LIF) *Journal of Anal.* Atomic Spectrom. 24: 1421-1428.

Maji S., Kumara S., Sundararajan K., 2021. Enhanced laser induced breakdown spectroscopy signal intensity in colloids: An application for estimation of Cu and Cr in aqueous solution. *Spectrochimica Acta Part B: Atomic Spectroscopy,* 175:106010.

Miziolek A.W., DeLucia F.C., Munson C.A., and Gottfried J.L. 2008. Recent Progress in LIBS-Based Technologies for Security Applications. *Laser Applications to Chemical, Security and Environmental Analysis Optical Society of America* LThC1.

Musazzi, Sergio, Perini, Umberto. 2014. Laser-Induced Breakdown Spectroscopy Theory and Applications. *Springer Series and Optical Sciences*. 182.

Nunes L., Braga J Trevizan L., De Souza P., De Carvalho G., Júnior D., Poppie R. and Krug F. 2010 . Optimization And Validation Of A LIBS Method For

The Determination Of Macro And Micronutrients İn Sugar Cane Leaves. *J. Anal. At. Spectrom*. 25: 1453-1460.

Jeff H., 2010. Short history of laser development. *Optical Engineering,* 49:9.

Palásti J., Albrycht P., Janovszky P., KarolinaPaszkowska K., ZsoltGeretovszky Z., GáborGalbács G., 2020. Nanoparticle enhanced laser induced breakdown spectroscopy of liquid samples by using modified surface-enhanced Ramann scattering substrates. Spectrochimica Acta Part B: Atomic Spectroscopy 166:105793.

Radziemski L. J., Cremers D. A. 1989. Laser Induced Plasmas and Applications, *Marcel Dekker,* New York 21(22) : 295-326.

Salajkova Z., Gardette V., Kaiser J., Dell'Aglio M.,C De Giacomo A., 2021. Effect of spherical gold nanoparticles size on nanoparticle enhanced Laser Induced Breakdown Spectroscopy. *Spectrochimica Acta Part B:* Atomic Spectroscopy. 179: 106105.

Senesi G.S., Dell'Aglio M., Gaudiuso R., De Giacomo A., Zaccone C., De Pascale O., Miano T.M., Capitelli M. 2009. Heavy Metal Concentrations İn Soils As Determined By Laser-İnduced Breakdown Spectroscopy (LIBS) With Special Emphasis On Chromium. *Environmental Research.* 109(4): 413-420.

Sezer B., Bilge G.,Boyaci I.H., 2017. Capabilities and limitations of LIBS in food analysis. TrAC Trends in Analytical Chemistry 9:345-353.

Simeonsson, J. B., and A. W. Miziolek. 1993. Time-Resolved Emission Studies of ArF Laser-Produced Microplasmas. *Applied Optics.* 32 (6): 993-947.

Skoog D. A., Holler F.J., Crouch S. R., 2007. *Principles of Instrumental Analysis* 6:142.

Stamplecoskie K. and Scaiano J. 2010. Light Emitting Diode Irradiation Can Control the Morphology and Optical Properties of Silver Nanoparticles. *J. Am. Chem. Soc*.132: 1825–1827.

St-Onge L., Kwong E., Sabsabi M., Vadas E. B. 2002. Quantitative analysis of pharmaceutical products by laser-induced breakdown spectroscop. *Spectrochimica Acta Part B:* Atomic Spectroscopy. 57(7): 1131-1140.

Tamaru H., Kuwata H., Miyazaki H., and Miyano K., 2002. Resonant light Scattering from individual Ag nanoparticles and particle pairs. *Appl. Phys. Lett.* 80: 1826.

Tzortzakis S .2006. Ultraviolet Laser Filaments For Remote Laser-İnduced Breakdown Spectroscopy (LIBS) Analysis: Applications İn Cultural Heritage Monitoring. *Optıcs* 31(8).

Unser S., Bruzas I., He J., Sagle l., 2015. Localized Surface Plasmon Resonance Biosensing: Current Challenges and Approaches. *Sensors*, 15:15684-15716.

Ünal S., Yalçın Ş. 2010. Development Of A Continuous Flow Hydride Generation Laser-İnduced Breakdown Spectroscopic System: Determination Of Tin İn Aqueous Environments. *Spectrochimica Acta Part B:* 65:750–757.

Viskup R., Wolf C., and Baumgartner W. 2020. Qualitative and Quantitative Characterisation of Major Elements in Particulate Matter from In-use Diesel Engine Passenger Vehicles by LIBS. *Energies.* 13: 368.

Wang W., Kong W., Shen T., Man Z., Zhu W., He Y., Liu F., 2021. Quantitative analysis of cadmium in rice roots based on LIBS and chemometrics methods. Environmental Sciences Europe 33:37.

Who , 2019 . Chromium in Drinking-water . Draft Background document for development of WHO Guidelines for Drinking-water Quality.

Yang F., Jiang L., Wang S., Cao Z., Liu L., Wang M., Lu Y. 2017. Emission Enhancement Of Femtosecond Laser-İnduced Breakdown Spectroscopy By Combining Nanoparticle And Dual-Pulse On Crystal SiO_2 . *Optics & Laser Technology.* 93: 194-200.

Zhao X., Zhao C., Du X., and Dong D. 2019. Detecting and Mapping Harmful Chemicals in Fruit and Vegetables Using Nanoparticle-Enhanced Laser-Induced Breakdown Spectroscopy. *Scientific Reports* . 9: 906.